Sedimentology, Age and Stable Isotope Evolution of the Kurnool Group, Cuddapah Basin

Cari N. Bertram
University of Adelaide
cari.bertram@student.adelaide.edu.au



Contents

Abstract

The Kurnool Group unconformably overlies the Cuddapah Supergroup in the Cuddapah Basin, one of several Proterozoic basins in India. Neither the Kurnool Group nor the origin of the basin in which it is deposited is well constrained. In order to better establish its depositional age and basin evolution, I have performed a combined sedimentological, geochronological and isotope geochemical study of the Banaganapalle Formation, Narji Limestone, Auk Shale, Panium Quartzite, Koilkuntla Limestone and Nandyal shale, from bottom to top respectively. This study used U-Pb and Hf isotope analyses on detrital zircons to constrain the maximum depositional age and provenance of the sediments. Carbon (C) and oxygen (O) stable isotopes constrained the depositional period for the Narji Limestone and Auk Shale. Stratigraphic analysis was used in conjunction with gamma ray spectrometry (GRS) U, Th and K data to determine the depositional environment. U-Pb zircon geochronology shows that the Kurnool Group is younger than 2516 ± 19 Ma sourced from a detrital zircon in the Banaganapalle Formation. Due to peak ages at 2514 ± 13 Ma from the Panium Formation and 2623 ± 27 Ma and 3167 ± 22 Ma in the Banaganapalle Formation is it clear that the sediments are sourced from the Dharwar Craton. A clear trend in O and C isotopes reveals that sediments were deposited sometime between the Mesoproterozoic to the Early Neoproterozoic in a sub-tidal environment. There is moderate petroleum potential for the Narji Limestone and it shows potential as a frontier basin.

1. Introduction

The crescent shaped Cuddapah Basin is the second largest Proterozoic basin in India. It is located in eastern Peninsular India and has an area of 44, 500 km^2 with a maximum width of 440 km. It is filled with 12 km of mixed carbonate-siliciclastic sediments and is intruded by minor igneous activity including dykes and sills. The basin is bound to the west and underlain by the Archean Dharwar Craton and to the east by the southern Eastern Ghats (Fig. 1). The Dharwar Craton comprises orthogneisses that are often referred to as 'Peninsular Gneiss', volcano-sedimentary greenstone belts and granitic intrusions. These all terminate at the basin boundary and had completed forming at the start of deposition. Deep seismic soundings have shown that the basin and the basement thicken eastward, towards the Eastern Ghats (Kalislam, 1976; Naganjaneyulu and Harinarayana, 2004).

The sediments in the Kurnool Group represent Neoproterozoic deposition which unconformably overlies the older Cuddapah Supergroup. The Cuddapah Supergroup is Meso- to Neoproterozoic in age (Crawford & Compston, 1972; Zachariah, 1999; Chakraborty, 2010) and is present throughout the basin whereas the Kurnool Group is only in two smaller sub-basins in the west and northeast of the basin (Fig. 2). This study focuses on all six formations in the Kurnool Group in the western Kurnool Sub-basin.

Two cycles of sandstone, limestone and shale make up the sediments in the Kurnool Group. This basin experienced multiple sequences of transgression and regression. From top to bottom the formations are Banaganapalle Formation (made up of conglomerates and sandstone), Narji Limestone, Auk Shale, Panium Quartzite, Koilkuntla Limestone and Nandyal Shale (Table 1). Currently there are no direct constraints on the Kurnool Group.

The Cuddapah Basin shows a considerable amount of outcrop that is also easily accessible. Considering this, the Kurnool Group is extremely poorly dated. No modern geochronology has been attempted in the basin and any absolute age constraints will significantly advance knowledge of the evolution of this part of India. At this stage, it is necessary to set up a foundation for future studies of the Kurnool Group. There is a lack of very basic information regarding the age of sediments, deposition and the evolution of the basin. The Cuddapah Basin is a frontier basin, and it has been overlooked as a possible petroleum source considering the limestone in the Kurnool Group. The aim of this study is to examine the depositional environment, confirm the age of the deposition and test whether the sediments are derived from erosion of the newly exposed Eastern Ghats or the underlying Dharwar Craton.

These objectives have been completed using stratigraphic logs that will be correlated with the carbon and oxygen isotope data from a stable isotope mass spectrometer and gamma ray spectrometry data collected in the field. In this study I am also presenting new geochronological U-Pb detrital zircon laser ablation - inductively coupled plasma mass spectrometer (LA-ICPMS) data and laser ablation - multi collector - inductively coupled plasma mass spectrometer (LA-MC-ICPMS) Hafnium (Hf) isotope data. The Hf isotope data is important as it will place additional constraints on the detrital zircon ages (Veevers et al, 2004; Andersen, 2005; Belousova et al, 2009; Howard et al, 2009). This data collection will constrain the maximum depositional age and examine the provenance of this section of the basin.

2. Geological Setting

The Dharwar Craton in Peninsular India consists mostly of Archaean continental crust. It is bounded to the east by the Cuddapah Basin and the Eastern Ghats. The minimum age for the tonalitic–trondhjemitic–granodioritic (TTG) basement is 3127 Ma (Jayananda, 2000). Of the three distinct terrains in the Eastern Dharwar Craton, the Peninsular Gneiss is the oldest ranging from 3000-3400 Ma (Meen et al, 1992; Peucat et al, 1993; Jayananda et al, 2000). The volcano-sedimentary greenstone beltscomprise two sequences: the older Sargur Group and the younger Dharwar Supergroup. These have been aged between 3000-2500 Ma (Anil Kumar et al, 1995; Radhakrishna & Naqvi, 1986; Raase et al, 1986; Taylor et al, 1984). A calc-alkaline to potassium rich granitic intrusion terminates the deformation in the Dharwar Craton. This intrusion has been dated at between 2500-2600 Ma (Rogers, 1986; Jayanada et al, 2000).

The Eastern Ghats belt is located to the east of the Cuddapah Basin and runs along the coast of Peninsular India. To the west it is bordered by Archaean continental crust, including the Dharwar Craton and the Baster Craton. Different deformation cycles have influenced the structure of the Eastern Ghats belt. It corresponds to a polycyclic granulite terrain which has undergone repeated high temperature metamorphism and deformation from the Proterozoic to the early Phanerozoic. The Krishna Province, which corresponds to the southernmost extension of the Eastern Ghats, is in direct tectonic contact with the Cuddapah Basin to which is forms its eastern borders. The Krishna orogens consist of three domains respectively from east to west: Ongole, Vinjamuru and Udayagiri (Fig. 1). The earliest deformation event to occur in the Ongole Domain was a calc-silicate rock intrusion of enderbitic to charnockite granulites between 1720 to 1704 Ma (Dobmeier & Raith, 2003; Dobmeier et al, 2006; Simmat & Raith, 2007; Upadhyay et al, 2009). High to Ultrahigh-temperature metamorphism

occurred in the Ongole Domain between 1650 and 1590 Ma (Simmat & Raith, 2008; Upadhyay et al, 2009). Localised ductile-brittle deformation and hydration occurred from 1450-1350 Ma (Simmat & Raith, 2008; Upadhyay et al, 2009) with a thermal overprint at ~1100 Ma (Simmat & Raith, 2008; Upadhyay et al, 2009). The Ongole Domain is thrust westward over the Vinjamuru Domain, which has a dominant lithology of granitic gneiss (Dobmeier et al, 2006; Mukhopadhyay & Basak, 2009). This was intruded by granitic magma which has identical U-Pb upper intercepts of 1588.4 ± 7.7 and 1589.7 ± 5.7 Ma that dates the emplacement (Dobmeier et al, 2006). The Udayagiri Domain consists of greenshist facies volcanosedimentary sequence which holds conglomerates, pelites and psammites with local intraclasts of cherts, limestones and felsic volcanics (Dobmeier & Raith, 2003; Vasudevan et al (in press), quoted in Dobmeier et al (2006)). Metavolcanic rocks have Pb-Pb zircon evaporation ages of 1868 ± 6 Ma and 1771 ± 8 Ma and this reflects the deposition age (Vasudevan et al (in press), quoted in Dobmeier et al (2006)). Little else is known about this domain.

Peninsular India is covered with Proterozoic sedimentary basins which are commonly known as the Purana Basins (Chaudhuri et al, 1999; Meert et al, 2010). There is no consensus as to how they have formed. Radhakrishna & Naqvi (1986) have studied these basins and believe that between 2000-1500 Ma these basins were formed from subduction and flexture at the eastern and northern margins of the Dharwar-Singhbhum Protocontinent. Chaudhuri et al (2001) believes that these basins were formed due to controls from pre-existing sutures and/or weak zones. It can be seen that these basins have a broad similarity to each other and in general represent shallow marine, epicratonic, passive margin sequences deposited in an extensional tectonic regime (Dasgupta & Biswas, unknown).

As for the Cuddapah Basin, there are many theories for it its creation. Pandey et al (1997) and Chatterjee & Bhattacharji (2001) agree that mafic dyke swarms Eastern Dharwar Craton are associated with thermal extension and fracturing of the crust which may have lead to its formation. An agreeing theory is where the basin geometry and evolution is primarily controlled by basin-marginal faults where the basin developed in a failed rift setting (Chadauri et al, 2002). Evidence of rifting is oscillatory movements which were shown by the variation from fluvial-shallow marine to slope-basin deposition. Singh and Mishra (2002) have proposed that the Cuddapah Basin was formed in a peripheral foreland basin setting due to eastward dipping continental crust under the eastern part of the Cuddapah Basin. An agreeing theory is that the Cuddapah Basin is a foreland basin due to its position close to the Eastern Ghats (Manikyamba et al, 2007) which had a higher tendency for crustal sagging (Raman and Murty (1997), quoted in Chakraborty et al (2010)). Although the Cuddapah Basin may have a foreland origin, Rogers (1986) is suggesting that the basin started off as circular, and was then deformed by the Eastern Ghats Orogeny to form the crescent shape which can be seen by the Nallamali Fold Belt.

The formation of the Kurnool sub-basin is less disputed than that of the Cuddapah Basin. The Kurnool basin is a distinct technostratigraphic unit from the Cuddapah Basin. Gravity-induced block faulting and subsidence were the triggers that caused the basin to form in a depocentre (in press Chakraborty, 2010). During deposition the Kurnool Group underwent subsidence controlled by deep faults, and strong local movements all of which varied during the cycles (Meijerink, 1984; Chakraborty, 2010). Post deposition there has been eastward thrusting movements of deep faults, epeirogenic movements and folding and metamorphism in the eastern parts of the basin (Chakraborty, 2010).

The Cuddapah Basin is situated in eastern Peninsular India and has an area of 44, 500 sq. km with the largest width at 440 km west to east. It contains ~12 km thick stratigraphy which is at its deepest at the east of the basin, which overlies over a 40km thick crust of the Eastern Dharwar Craton (Kalislam, 1976; Naganjaneyulu and Harinarayana, 2004). Structures in the sediments show that they may be derived from the south and west (Murthy, 1976, as quoted in Dasgupta et al, 2005). Madhava Rao & Gokhale (1973) have also observed through ripples that current is from the west to east in the Banaganapalle Formation, which is consistent with the sediments being sourced from the Dharwar Craton. In the western part of the basin the sediments are generally unmetamorphosed, except for parts of the Kurnool Group, whereas in the eastern part they show deformation in the form of the Nallamali fold thrust belt (Chakraborty, 2010; Meijerink, 1984).

The basin is suspected to be of Palaeoproterozoic age, with deposition occurring from the Palaeoproterozoic to the Neoproterozoic. Age constrains for the age of deposition of the Kurnool Group formations come from the underlying Cuddapah Supergroup as well as within the Kurnool Group. The youngest Cuddapah Supergroup formation is the Cumbum Formation which is in the Nallamali Group and this underlies the Kurnool Sub-basin (Table 1). This has been dated using detrital zircons and yielded a $^{206}Pb/^{238}U$ age of 913±11 Ma (unpublished data by Mackintosh, 2010). This constrains the maximum depositional age for the Kurnool Group. The Cuddapah Basin is said to be mid-late Proterozoic in age, due to a lack of any known Phanerozoic body-fossils/floral impressions within the formations (Gupta, 1998). Kimberlite and lamproite pipes are cross-cutting the underlying sediments of the Cuddapah Supergroup, and the pipes show ages younger than 1090 Ma or 1140 Ma from Rb-Sr and K-Ar dating (Crawford & Compston, 1972; Chaudhuri et al, 1999; Chakraborty, 2010). Chalapathi Rao et al. (1995) have dated lamporite which lies in the Cuddapah Basin

with K-Ar methods at 1350-1380 Ma which may indicate a second magmatic event as it was previously thought that there was only one magmatic event. This is significant because the Banaganapalle Formation is diamondiferous and this composition is most likely a result of the weathering of the pipes. Carbonaceous megaremains in Auk Shale have been dated as Neoproterozoic in age (Sharma & Shukla, 1999). There are carbonaceous impressions and compressions in the bedding planes of the boundaries between the siltstone and the shales, and the shale to claystone (Sharma & Shukla, 1999). There are five megaremains which are *Chuaria circularis*, *Tawid* remains, *Ellypsophysid* remains, *Moranid* remains and *Beltinid* remains (Sharma & Shukla, 1999).

3. Methods

3.1 LA-ICPMS Geochronology

LA-ICPMS geochronology was undertaken to determine the age of detrital zircon. Samples were chosen for geochronology based upon their relative location, sample 'freshness' and perceived potential for detrital zircons, i.e. sandstones. These samples were crushed, coarsely milled using a tungsten-carbide mill and sieved with the 75-425 μm fraction retained for zircon separation which involved hand panning and hand held Nd magnets and the zircon grains were then handpicked and mounted in a 1 inch epoxy disc. The disc was polished so the zircons were half their depth and imaged using backscatter electron (BSE) and cathodoluminescence (CL) using a Phillips XL-20 with attached Gatan CL located at Adelaide Microscopy, University of Adelaide.

The U-Pb detrital zircon geochronology was undertaken using an LA-ICPMS located at Adelaide Microscopy. Data was acquired using a New Wave 213 nm Nd-YAG laser in a He

ablation atmosphere, coupled to an Agilent 7500cs ICP-MS. The LA-ICPMS operating procedures are set up similarly to Payne et al. (2006). ^{206}Pb, ^{207}Pb, ^{208}Pb, ^{232}Th and ^{238}U were analysed with ^{235}U calculated from ^{238}U using a $^{238}U/^{235}U$ ratio of 137.88. ^{204}Pb has Hg interferences on the LA-ICPMS so an offline integration of the signal was used to select the part of the signal which was common Pb free this can be used to assess the validity of the results. An external zircon matrix-matched standard GJ-1 (TIMS normalisation data $^{207}Pb/^{206}Pb$ = 608.3 Ma, $^{206}Pb/^{238}U$ = 600.7 Ma and $^{207}Pb/^{235}U$ = 602.2 Ma, Jackson et al, 2004) was used to correct for mass bias and fractionation in combination with the Plešovice zircon standard (concordant U–Pb age with a weighted mean $^{206}Pb/^{238}U$ date of 337.13 ± 0.37 Ma, Sláma, 2008) to monitor data quality. Isotopic analysis software Glitter (version 0.4) was used to process raw data (Griffin et al, 2008). Concordia diagrams and probability distribution curves where constructed using the ISOPLOT macro (Ludwig 2000). The concordancy was calculated by dividing the $^{207}Pb/^{206}Pb$ age by the $^{206}Pb/^{238}U$ age and the $^{207}Pb/^{206}Pb$ age was used. The GJ-1 standard had a $^{206}Pb/^{238}Ub$ weighted average of 601.0±1.6 (95% conf., n = 92, MSWD = 0.28). The Plešovice zircon standard was used to monitor data quality, which produced a $^{206}Pb/^{238}Ub$ weighted average of 343.6±4.0 (95% conf., n=26, MSWD=4.5).

3.2 In-situ zircon Hf isotope LA-MC-ICPMS

In-situ Hf isotope data was collected with a Thermo-Scientific Neptune Multi Collector ICP-MS coupled to a New Wave UP-193 Excimer laser (193nm) at Waite Campus, University of Adelaide, Adelaide, following procedures of Payne et al. (in prep). The samples analysed were two of the three used for LA-ICPMS analysis. Concordant zircon grains (90-110% concordance) were analysed in the same domain as they were for U-Pb LA-ICPMS

geochronology. The laser conditions were 4ns pulse length, 5 Hz with a 50 um spot size (~10J/cm^2). The ablated material travelled through a He ablation atmosphere mixed with Ar sample gas. Set-up of the system prior to ablation sessions was conducted using analysis of JMC475 Hf solution and an AMES Hf solution. ^{171}Yb, ^{173}Yb, ^{175}Lu, ^{176}Hf, ^{177}Hf, ^{178}Hf, ^{179}Hf and ^{180}Hf were measured on Faraday detectors with $10^{12}\Omega$ amplifiers and an integration interval of 0.232 seconds. Hf mass bias was corrected using exponential law fractionation correction using a stable Hf isotope ratio of ^{179}Hf/^{177}Hf=0.7325.

Yb isobaric interference on ^{176}Hf was corrected by direct measurement of Yb fractionation using ^{171}Yb/^{173}Yb coupled with the Yb isotopic values of Segal et al. (2003). The applicability of these values were verified by analysing JMC 475 Hf solutions doped with varying levels of Yb with interferences up to ^{176}Yb/^{177}Hf= ~0.5. Lu isobaric interference on ^{176}Hf corrected using a ^{176}Lu/^{175}Lu ratio of 0.02655 (Vervoort et al., 2004) assuming the same mass bias behaviour as Yb. For Yb signals below 10 mV interference corrections were made using an empirically derived ^{176}Yb/^{173}Yb ratio and the Hf mass bias factor similar to the method described by Griffin et al. (2000). This was done as the potential errors involved in the method are outweighed by the significantly greater uncertainty caused by the small Yb beam. In this case an empirically derived ratio of 0.739689 was used. This was derived by analysis of a series of Yb and Hf doped glass beads. Interferences from REE may affect the data. ^{160}Gd^{16}0 and ^{160}Dy^{16}0 both add up to 176 so there may be an overcorrection for Yt and Lu. If the ^{176}Lu/^{177}Hf ratio is above 0.1, the value will be discarded. Confirmation of accuracy of the technique for zircon analysis was monitored using a combination of the Plešovice, Mudtank and QGNG standards. Crustal model ages (T^C_{DM}) were calculated for each zircon

assuming average continental crust with $^{176}Lu/^{177}Hf$ values of 0.0015 (Griffin et al, 2002) as the zircon grain growth reservoir.

3.3 Stable Isotopes Geochemistry

Carbonate hand samples were collected approximately every 5 metres in the course of measuring stratigraphic sections. Carbonate samples were cut to expose a clean surface, which was then drilled to produce a fine powder. δ13C and δ18O isotope data were acquired simultaneously on a Micromass Isoprime dual inlet mass spectrometer at L'Université du Québec à Montréal. Approximately 100 µg of powder was reacted in singular glass reaction cells with purified H3PO4 at 90 ºC for 10 minutes while being constantly cryogenically trapped. Evolved CO2 was cryogenically distilled then measured against an in-house reference gas. Both δ13C and δ18O samples were calibrated to VPDB using an in-house calcite standard. All δ13C and δ18O are reported with respect to the Vienna Pee Dee Belemnite (VPDB) as per mil deviations.

3.4 Sequence Stratigraphy

Sequence stratigraphy is important for detailed depositional and sedimentary observations in the Kurnool Group using the accessible outcrop. The three transects were done: 1) from the Banaganapalle to the top of the Narji Limestone 2) from the Narji Limestone to the Panium Sandstone and 3) through the Auk Shale to the Panium Limestone (Table 1). The total lengths of these sections were 65.5m, 124.4m and 73.6m respectively. The location for the logged sections was chosen on accessibility, length (known or possible), and sediments. The location of each of the sections is in Table 2. Stratigraphic logs were created to compare the intervals over different locations as well to provide as a detailed look at the relationships between

formations. Th, U and K concentration were acquired every 5 metres using a hand-help gamma ray spectrometer.

3.5 Issues and Potential Errors

Contamination is the highest risk when using samples that are not whole rock. Action was undertaken to prevent contamination of the sample such as cleaning labs before and after preparation, and cleaning any machinery such as the rock crusher, diamond saw and drill bit before and after using them. An error which may not be accounted for is human error when using the equipment in Adelaide Microscopy and when organising data. There could also be an issue with the LA-MC-ICPMS and LA-ICPMS not properly tuned or set up for zircon analysis. Standards are used in conjunction with the sample. Generally the sample shows the same age over the grain(s) but in some cases there are areas of the grain which are more accurate than other areas. If the incorrect part of the grain was used as a standard it may throw the results out but not to any great consequence. Undetected interferences from REE in the LA-MC-ICPMS and LA-ICPMS might pose an issue on corrections made based on the amount of elements detected.

4. Stratigraphy

4.1 Facies Descriptions

4.1.1 Cross Bedded Sandstone

This facies makes up most of the Banaganapalle Formation and typically consists of a fine to medium grained quartz arenite. Rocks in this facies are usually brown in colour and contain well rounded grains. Isolated clasts are sporadic through parts of the observed facies (Fig. 3a)

and they are sub rounded to rounded and no larger than 2 cm in diameter. There are distinct laminations, and as the laminations are up to 2 cm thicker as the grains coarsen (Fig. 3b). Cross bedding and trough cross bedding (Fig. 3c and 3d respectively) at both a scale of 20 cm and a scale of 5 cm are very common. These had a varied direction as expected; they included dip/dip directions of 31/148 and 18/267 (Table 3). Ripples appear on some surfaces and these may change from a 3 cm wavelength on one surface to a 10 cm wavelength on only 30 cm apart vertically adjacent surfaces. Four sets of ripples seen in the observed sections of the sandstone in the Banaganapalle Formation. These values can be found in Table 3. This formation can be seen in the *Narji 2* stratigraphic log before the transition into the Narji Limestone (Fig. 6).

4.1.2 Carbonate Mud Shale

The carbonate mud shale lies in the transition zone between Banaganapalle Formation and the Narji Limestone. This can be seen between 0 and 8.8 m on the *Narji 2* stratigraphic log (Fig. 6). It is ~8 m of carbonate shale, which is composed of sandy and muddy layers.

4.1.3 Carbonate Cemented Sandstone

This facies represents the base of the Narji Limestone. Here are cross bedding and intraclasts (Fig. 3e), although they do not co-exist in the sections observed. Further up in this facies it transitions into ribbons (Fig. 3f) with some pyrite inclusions, hummocky cross stratification (HCS) (Fig. 3g) and thick bedding with clay beds and fine laminations. The positions of these sedimentary features can be seen in the *Narji 1* and *Narji 2* stratigraphic logs (Fig. 5 and 6 respectively). The pyrite inclusions are 5 mm - 10 mm across. The clay beds are 0.5 to 1cm thick and contain pockets of sand (Fig. 3h). There are low angle truncations and dolomitised

regions, as well as intermittent chert layers approximately 15m apart. The bedding is thinning from 2cm to 5mm as the formation goes up.

4.1.4 Grainstone

In the middle fo the Narji Fomration the limestone can be defined as a grainstone (Fig. 3i). This has thin bedding and <1mm grainsize. Within the grainstone there are stylolites between the thick bedding. The grainstone is dark grey in colour due to a high amount of organic matter, and stylotisation occurs about every 10cm. These sedimentary features can be seen in the *Narji 1* and *Narji 2* stratigraphic logs (Fig. 5 and 6 respectively). Pyrite crystal inclusions are between ~1mm to ~5mm across.

4.1.5 Shaley Limestone

This limestone is present at the top of the Narji Formation. It may be a transitional boundary between the Narji Formation and the Auk Shale. This facies shows quite shaley bedding with 2 cm to 5 mm thick beds. It then transitions into suspension bedding which shows suspended layers of sand and mud ~1.5 cm thick to 5 mm thick and alternating. Pyrite is small, and limestone is dark in colour.

4.1.6 Calcareous Shale

This facies makes up the Auk Shale formation. It can be defined by shales trending from 2 cm thick grey mud beds to carbonate rich beds to more pale grey/greeny non-calcareous beds. It is a highly weathered outcrop. Beds are approximately 1cm thick and do not change over the interval. There is a sharp boundary between the carbonaceous shale and the massive sandstone, which can be seen in the *Narji 1* and *Auk* stratigraphy logs (Fig. 5 and 7 respectively).

4.1.7 Massive Sandstone

This facies makes up the Panium Quartzite. Generally this facies is defined as a fine to medium grained sandstone which shows no grading (Fig. 3k). It is a pure, grain supported fabric with very little matrix. The grains are sub angular to rounded, and the rock weathers the same. There is one area which shows 1m scale cross bedding and pinching and swelling but this is very uncommon as it is mostly massively bedded. This can be seen in the *Auk* stratigraphy log (Fig. 7). Lenses of shale and clay appear close to the boundary between massive sandstone and calcareous shale in one observed transect.

4.1.8 Clay-Rich Limestone

This facies makes up the Koilkuntla Limestone. Only 3 m of this facies was observed and that showed a rock which is light in colour, with small laminations up to 1cm, and large bedding from 5-20cm. It is highly weathered and therefore outcropping is not common. This limestone is more clay rich than the Narji Limestone.

4.1.9 Mud-Rich Shale

This facies represents the Nandyal Shale. The facies observed is characterised by well laminated, fine purple/brown beds (Fig. 3l). It is slightly calcareous and rich in clay, and highly weathered. There are silty coarser beds between the mud beds and it did not show much significant change over the observed interval.

4.2 Palaeogeography

4.2.1 Banaganapalle Formation

The Banaganapalle Formation unconformably overlies the Cuddapah Supergroup. The top of the Cuddapah Supergroup is the Nallamali Formation, which holds shales, quartzite and slate. The lower section of the Banaganapalle Formation is a conglomerate made up of rip-up clasts of the underlying formation. Diamondiferous lamporite pipes run through the Nallamali Group, and the Banaganapalle Formation also has diamondiferous clasts in the conglomerate which are from the underlying formation. This shows a high energy environment as the underlying formation was ripped up.

Another indication of a high energy environment are symmetric large and small ripples which are vertically juxtapositioned where the larger ripples lie on top of the smaller ones. This may suggest deepening water, due to tectonics or sea level change. This is also indicative of increased flow strength conditions. The sediment is mature and this implies a beach environment.

The palaeocurrent direction for ripples is approximately east/west with minimal dipping. Evidence for this is four sets of ripples seen in the observed sections of the sandstone in the Banaganapalle Formation. These values can be found in Table 3. Cross bedding was also seen and this has a more varied direction, as expected. The dip/dip direction for those include 31/148 and 18/267.

There is a transitional boundary between the Banaganapalle Formation and the Narji Limestone. There is ~8 m of carbonate mud shale between them, with sandy and muddy layers suggesting a swash zone. At this time there might be a barrier preventing sediment

coming in, or a change in energy which is why there is a change to limestone and a higher carbonate input. The source could be shut off due to orogeny cycles and a lack of sediment being deposited. This formation is the transition into a transgressive sequence in this part of the basin.

4.2.2 Narji Limestone

At the edge of the calcareous mud shale and at the base of the Narji Limestone there are two observed environments. In one part of the basin there were intraclasts present which is evidence of a storm environment. Previously this would have been a mud as it is very thinly bedded and there are layers of sand and clay and pockets of mud throughout the limestone. This could be part of the transitional period which was then ripped up by storm waves. In other parts of the basin where the transition could be seen from Banaganapalle to Narji there was no evidence for any reworking of the seabed which shows that there were local storms during this depositional period. This section is generally deepening due to the decrease in clay and sand. As is it getting deeper there are ribbons forming which have then been affected by storm waves. HCS is also visible in the carbonate cemented sandstone further up in the sequence as it transitions from storm currents to fair-weather currents. These beds are of varying thickness and show clay in between beds, which implies moderate to high energy shallow sub-tidal conditions. This then transitions into a grainstone and then a dark shale. Pyrite is visible through the formation which shows a reducing iron environment.

At the top of the formation there are multiple stages of suspension bedding where it cycles between suspended and settled clay and mud which is a deep water depositional environment. At this stage there may have been a break in the barrier which was holding back sediments, or a decrease in seawater and it has therefore started to transition into a regressive environment

with increased sediment supply/less water. There is also a high amount of pyrite which relates to the increased reduced iron enrichment.

4.2.3 Auk Shale

The Auk Shale formation was progressively a more storm based environment. There are 1 cm thin parallel mud beds at the base of the formation, with some clastic input. This implies intermittent sediment supply and quiet waters. The beds then become more calcareous and slightly thicker layers (~2 cm). This bedding was also parallel and silt was between the beds in some areas. A weak storm wave base could be the force for this environment where the pulses of sediment supply are longer than the previous sedimentation. This then moved to silty shale which has been oxygenated so this would be shallower than the previous deposition. This sediment and bedding continued until the Panium Quartzite where there was a very sharp boundary.

4.2.4 Panium Quartzite

In two different parts of the basin there were different conditions for the boundary between the shale and the sandstone. Where there is cross bedding and thin 5 mm laminations as well as a few layers of shale and pockets of clay there was also little matrix and this suggests a shallow-marine environment with storm erosion from the lower Auk Shale and sediment flows. Here the direction of the cross beds were east/south east. In other sections of the basin where there is massive bedding, mature sediments, and a lack of sedimentary features, this may have been a beach environment. This regressive stage might have been halted by another sediment barrier.

4.2.5 Koilkuntla Limestone and Nandyal Shale

The Koilkuntla Limestone was formed in a calm environment which can be seen from the thin 5 mm laminations. This laminated section is thick, and holds a lot of clay and manganese. This environment would have formed after a barrier stopped silisiclastic sediments from deposition. The Nandyal Shale formation has very thin horizontal bedding, fine grained, clay rich and this suggests it was potentially deposited as tidal flats, although no mud flats were observed. These formations are not able to be put in context we well as the other formation due to no boundaries observed between the formations.

4.3 Geophysical Logs

Three transects were undertaken through different sections of the Kurnool Group (Table 2) and the values for these are found in Table 4. The GRS data was collected whilst logging and K, U and Th and total dose of elements were recorded. K correlates to the amount of clay present in the rocks, due to the high K in clay. U and Th are close in the periodic table and therefore when Th is recorded it may actually be responding to U and vice versa. However, if the machine is calibrated correctly, this should not be a problem. When rocks weather they will produce Th and this will then lead to a higher reading of Th than primary values which will skew the data. When selecting an area of rock to log, weathered areas were eliminated. The GRS data will show radioactivity as well as sequence changes. Shales at maximum flooding surfaces will show a strong positive GRS total value due to radiogenic highs made up of elements which have been collected from the water column during this part of deposition.

There is a maximum total value of 4 in the grainstone, which also correlates with the *Narji 2* log (Fig. 6). Th has a maximum of 1.4 ppm at the same level as the total maximum value and

shows the same trend as the *Narji 2* log (Fig. 6). The *Narji 2* geophysical log shows a total high of 30, with a K value of 0.6 % and Th value ~8 ppm (Fig. 6). This is about 5 m into the calcareous shale of the Auk Formation. At the top of the Narji formation there are higher values of total, K and Th than along the rest of the log. The *Auk* geophysical log has a maximum total value of 85, with a K value of 3%, U value of 0.2 ppm, and a Th value of 15 (Fig. 7). These high values may relate to a higher elemental concentration due to collection from the water column.

The *Narji 1* geophysical log shows No K or U values at all (Fig. 5). However, this is surprising as it was expected that the cross bedded sandstone might have higher values for U as the Eastern Ghats have average levels of U from the metamorphism. In the calcareous shale and the mud-rich shale there were Th/U ratios of 10-20. One GRS log in the silicate limestone yielded a Th value of 27.1 ppm, and a U value of 0.4 ppm. The Th/U ratio is 67.8. A GRS log in the calcareous shale yielded U values of 0.2 ppm and Th values of 14.7 ppm which totals a Th/U ratio of 73.

5. Results

5.1 LA-ICPMS U-Pb Geochronology

5.1.1 Sample CU10-05

This sample is from the upper sandstone section of the Banaganapalle Formation, which is before it transitions into the Narji Limestone. The sample is from the upper part of the section, just above a thin ~5cm layer of storm clasts. The grains are rounded and frosted, and

the sample has little matrix. The sample is indicative of a transgressive depositional environment. Out of the 22 analysed detrital zircon grains 11 were 100 ± 10% concordant. The concordant $^{207}Pb/^{206}Pb$ ages range from 2516.1± 18.73 Ma to 3389 ± 17.5 Ma (Fig. 8a). Within the concordant data there are no statistically valid clusters (Fig. 8b). The youngest $^{207}Pb/^{206}Pb$ age for this sample is 2516.1± 18.73 Ma with 110% concordancy.

5.1.2 Sample CU10-06

This sample is also from the upper section of the Banaganapalle Formation, and it is 10m higher stratigraphically than sample CU10-05. The main characteristics of this sample are rounded grains with little matrix. Out of the 58 detrital zircons that were analysed, 10 were 100 ± 10% concordant. The concordant $^{207}Pb/^{206}Pb$ ages of this sample range from 2542.1 ± 17.71 Ma to 3316.1 ± 16.1 Ma (Fig. 8c). There are two main populations of zircons. On the probability density distribution plots there is one population at 2623 ± 27 Ma (95% conf., n=2, MSWD=0.02) and another older group at 3167 ± 22 Ma (95% conf., n=2, MSWD=0.27) (Fig. 8d). Since there are only 10 concordant grains, the peaks look more significant than they really are. The youngest concordant age is 2542.3 ± 17.71 Ma with 96% concordancy.

5.1.3 Sample CU10-22

This sample is from the Panium Quartzite, which is in the middle of the Kurnool Group. It is a pure quartzite with a medium sand grain and very little to no matrix. The sample is 18m above the boundary between the Auk Shale and the Panium Quartzite and it represents the start of the shallowing water level of the basin. Forty zircon grains were analysed and 26 were 100 ± 10% concordant. The concordant detrital zircon $^{207}Pb/^{206}Pb$ ages of this sample range from 2060.9 ± 22.38 Ma to 3397 ± 16.9 Ma (Fig. 8e). There is a peak age at 2514 ± 13 Ma (95% conf., n=17, MSWD=2.6) where the main concordant population lies (Fig. 8f).

There are two younger grains. One has a concordant $^{207}Pb/^{206}Pb$ age of 2161.7 ± 19.1 with 104% concordancy and the youngest concordant $^{207}Pb/^{206}Pb$ age is 2060.9 ± 22.38 Ma with 98.4% concordancy.

5.2 In-situ zircon Hf isotope LA-MC-ICPMS

In-situ zircon Hf isotope analysis was conducted on 2 samples, CU10-05 and CU10-22, from the Banaganapalle Formation and Panium Quartzite respectively. Hf isotope data is reported in Table 6.

Eleven zircon grains with 100 ± 10% age concordance were analysed from sample CU10-05. Of these, 3 zircon grains yielded $^{176}Yb/^{177}Hf$ ratios above 0.1, and hence are not included in this discussion. The remaining grains yield ε_{Hf}^{T} values ranging from + 0.4 to +18.3 at the crystallisation ages of 2500 - 3400 Ma (Fig. 9). Crustal Depleted Mantle model ages (T^{C}_{DM}) calculated using $^{176}Lu/^{177}Hf$ values of 0.0015 yield ages of 2.29 – 3.67 Ga (Fig. 10). Eighteen zircon grains with 100 ± 10% age concordance were analysed for sample CU10-22. Of these two grains are not in this discussion due to $^{176}Yb/^{177}Hf$ ratios above 0.1. The remaining grains yield ε_{Hf}^{T} values ranging from -6 to +3.4 at the crystallisation ages of 2060 - 3250 Ma (Fig. 9). T^{C}_{DM} yielded ages of 2.50 – 3.59 Ga (Fig. 10). Both Banaganapalle and Panium samples $^{176}Hf/^{177}Hf$ values are highly variable ranging from 0.2807 to 0.2813 and 0.2814 respectively. Although all the values plotted on the graph are valid, I am disregarding any above the depleted mantle normalised curve.

5.3 Carbon and Oxygen Stable Isotopes

Carbon and oxygen stable isotope sections where constructed for two sections. This data can be found in Table 7. The Narji Limestone has excellent exposure and accessibility and it was

not difficult to sample. Two transects were sampled through the Narji Limestone, with one in the same area as the *Narji 1* stratigraphy log and the second one only for sampling. In the first transect the $\delta 13C_{carb}$ profile is fairly scattered ranging from +0.2 to +2.5 ‰ and slowly increasing as depth decreases (Fig 11). The $\delta 18O_{carb}$ from the same transect ranges between -12.3‰ and -6.8‰ and then back to -10‰ shows more of a trend (Fig 11). The second set of data is from Govindinne Quarry (15º 24' 3.9" N, 78º 12' 26.5" E) and it is 7.5 m long. This shows a $\delta 13C_{carb}$ profile that is slowly decreasing from +2.4 to +1.45 ‰ (Fig. 12). The $\delta 18O_{carb}$ values range from -9.3 to -10.83 ‰ and they also decrease as it gets higher (Fig. 12).

An sub-tidal environment formed the carbonates in the Narji Limestone. A lack of water movement means that these carbonates would most likely reflect a restricted inorganic environment. Diagenesis should be considered when interpreting $\delta^{13}C_{carb}$ and $\delta^{18}O_{carb}$ values as it can change the values from the primary depositional values (Halverson et al. 2007). Meteoric or hydrological fluids affect $\delta^{18}O_{carb}$ before it affects $\delta^{13}C_{carb}$ (Frank et al, 2003; Bartely et al, 2001). If the rock has been affected then there will be a covariant trend of sharply decreasing $\delta 18C_{carb}$ with a decreasing $\delta^{13}C_{carb}$, which can be shown by a $\delta^{18}O_{carb}$ vs. $\delta^{13}C_{carb}$ plot. From Fig. 14 we can see that there is correlation between $\delta^{18}O_{carb}$ and $\delta^{13}C_{carb}$ therefore it has been affected by diagenesis. Due to diagenesis, it means that the $\delta^{18}O_{carb}$ values are more likely to have measured burial temperature rather than relative seawater values. The confidence of this data is limited due to the digenesis, and the short transect. With this in mind, the $\delta^{18}O_{carb}$ values will not be included, as disgenesis affects O isotopes before it affects C isotopes.

6. Discussion

6.1 Age Constraints of Sedimentation in the Kurnool Sub-Basin

The Kurnool Group is thought to be Neoproterozoic in age. Previously the only age constraints available have been from fossils (Gupta, 1998; Sharma & Shukla, 1999) and age constraints from the Cuddapah Supergroup (Crawford & Compston, 1972; Chalapathi Rao et al, 1995; Chaudhuri, et al. 1999; Chakraborty et al, 2010; Mackintosh, 2010). Sediments from the Banaganapalle Formation, Panium Formation and Narji Limestone have been dated using detrital zircon U-Pb ages, and O and C stable isotopes.

U-Pb detrital zircon dating of the Banaganapalle Formation produced a maximum depositional age of 2516 ± 19 Ma. This shows that the Kurnool Group is younger than the Archaean. It does not provide a good constraint of the deposition of the Kurnool Group as there are no other igneous events which can constrain it further.

Carbon and oxygen stable isotope data from carbonate facies in the Narji Formation has provided data for the time of deposition. From the data showing a shift in $\delta^{13}C_{carb}$ values from ~ 0 ‰ to +2.5 ‰ we can deduce that the carbonates were deposited in the isotopically subdued area in the Mesoproterozoic to the Early Neoproterozoic (Kah et al, 1999; Frank et al, 2003). Due to limitations in collecting data there could not be a more precise time width. Further studies including strontium (Sr) isotopes will advance this knowledge.

6.2 Deposition of the Kurnool Group

The sediments in the Kurnool Group go from conglomerate to two cycles of sandstone, limestone and shale. This represents two transgressional/regressional events caused by sediment barriers, a reduction in energy, lack of sedimentation or rise and drop in sea level. It

is still uncertain which of these scenarios can be agreed upon given the data available. The deposition relates to a sub-tidal environment due to the deepening water and a trend from a beach environment to a deepwater environment and back to a beach setting from the Banaganapalle Formation to the Panium Formation. Very little is known about the nature of the boundary between the Panium and the Koilkuntla Limestone and the relationship between the Koilkuntla Limestone and the Nandyal Shale.

In relation to the spatial disposition there is a possibility that the sediments are not vertically adjacent. Due to the nature of the Koilkuntla Limestone and the Nandyal Shale, it is possible that parts of the Kurnool Group were deposited laterally, where the Panium and the Koilkuntla are horizontally adjacent along the sub basin, with a transition into the overlying Nandyal Shale. The quartzite would represent shallow areas of the basin, where as the limestone would represent distal areas.

6.3 Provenance of the Kurnool Group Sediments

The provenance of the Kurnool Group sediments was found using detrital zircon U-Pb and Hf isotope data and U, Th and K data collected in the field

The maximum depositional ages from the Banaganapalle Formation suggest that the sediments are sourced from the Dharwar Craton. Out of the two Banaganapalle samples the maximum depositional ages were 2516 ± 19 Ma (CU10-05) and 2542.3 ± 17.71 Ma (CU10-06). These ages are most likely from the Dharwar Craton, sourced from the volcano-sedimentary greenstone belts (3000-2500 Ma, Taylor et al, 1984; Raase et al, 1986; Radhakrishna & Naqvi, 1986; Anil Kumar et al, 1995) or the cal-alkaline to potassium rich granitic intrusion (2500-2600 Ma, Rogers, 1986; Jayanada et al, 2000).

The Panium Quartzite shows a group of zircon grain U-Pb ages at around 2500 Ma, and two younger zircon grain U-Pb ages at 2060.9 ± 22.38 Ma and 2161.7 ± 19.1 Ma. The Dharwar Craton shows a U-Pb age for the greenstone belt between 2600 – 2500 Ma (Ramakrishnan & Vaidyanadhan, 2008) and this data suggests that the greenstone belt is the source region for a high amount of the sediment in the Panium Quartzite. This may also relate to the other Rb-Sr age at 2.5 – 2.4 Ma age of the Mahbubnagar dyke swarm. The two younger ages may also be from the Mahbubnagar dyke swarm. From this data it is clear that the Banaganapalle Formation and the Panium Quartzite are most likely sourced from the Dharwar Craton.

Additional constrains on the source of sediments can be provided with Hf isotope data (Andersen, 2005; Howard et al, 2009; Veevers et al, 2004; Belousova et al, 2009). Hf isotope data was yielded from samples of the Banaganapalle Formation and the Panium Quartzite. The ε_{Hf}^{T} values range from + 0.4 to +18.3 at the crystallisation ages of 2500-3400 Ma for sample from the Banaganapalle Formation (Fig 10). The Panium Quartzite sample has a mixed source, as some ε_{Hf}^{T} values cluster near the CHUR normalised curve (-6 to +3.4 at the crystallisation ages of 2060 - 3250 Ma) and with scattered values closer to the depleted mantle normalisation curve (Fig. 10). $^{176}Hf/^{177}Hf$ zircon grains from both samples are characterised by 3.2 to 2.6 $T^{c}_{(DM)}$ crustal evolution lines (Fig. 11). This shows that there is juvenile and evolved input with major crustal reworking between 3.2 and 2.6 Ga.

Pre-existing Hf isotope and Nd data for the Eastern Ghats and Dharwar Craton can correlate this Hf isotope data with possible source regions. Zircons from the metapelites in the Eastern Ghats Belt lie between 2.7 and 1.9 crustal evolution lines indicating late Archaean to Mesoproterozoic juvenile provenance with major crust formation between 2.7 and 1.9 Ga (Upadhyay, 2009). Metasediments in the Ongole Domain of the Eastern Ghats have Nd

model ages of 2.6 to 2.8 Ga, which are similar to the adjoining Dharwar Craton granitoids (Rickers et al, 2001). It is expected that the Dharwar Craton would show an evolved terrain with Nd and Hf isotope values near the CHUR normalised curve and also areas of juvenile terrain where there has been mantle activity, whereas the Eastern Ghats (Ongole Domain) will show an evolved domain with negative ε_{Hf}^{T} values, and not much juvenile terrain. In relation to possible events which may have produced zircons, The Dharwar Craton and Eastern Ghats both have very different zircon-forming event ages. The minimum age of the Dharwar Craton tonalitic–trondhjemitic–granodioritic basement is 3127 Ma. As well as this, the Peninsular Gniess is aged between 3000 – 3400 Ma (Meen et al, 1992; Peucat et al, 1993; Jayananda et al, 2000). In the significant parts of the Eastern Ghats (Ongole, Vinjamuru and Udayagiri Domains) event ages range from 1868 ± 6 to ~1100 Ma (Simmat & Raith, 2008; Upadhyay et al, 2009; Vasudevan et al, (in press), quoted in Dobmeier et al, (2006)).

Considering all the data collected for the Banaganapalle Formation are all above the CHUR normalised curve, these grains are showing an Hf isotope signature similar to that of the Dharwar Craton. The Panium values are more scattered but these Hf isotope values reflect the Dharwar Craton composition due to a mixed source of high crustal depletion as well as juvenile input. Since the $T^{c}_{(DM)}$ are 3.2 to 2.6 this shows that it is too old to have been formed in the Eastern Ghats. The Dharwar Craton appears to be the source terrain due to older zircon-forming events.

Nd-model ages calculated for the Eastern Ghats have shown that there is an older group from 2.9 to 3.9 Ga (Rickers et al, 2001). This is said to represent the granitoids from the Dharwar and Eastern Indian Cratons and orthogneisses from the Eastern Ghats Belt. This shows that

although the ages that have been yielded show distinctly Dharwar Craton ages, they may still be sourced from the Eastern Ghats terrain.

Evidence from ripples in the Banaganapalle Formation suggest that water was flowing east and west as only symmetric ripples were visible (Table 3). This agrees with Madhava Rao & Gokhale (1973) who have also observed that the current was from the west to east due to ripples in the Banaganapalle Formation, which is consistent with the sediments being sourced from the Dharwar Craton.

Th, U and K GRS data was acquired through the Kurnool Group and has yielded data on the properties of this group (Table 4.). The Eastern Ghats generally has an average value for U found in metamorphic rocks and a high Th value due a terrain rich in monazite (Barker, 2010). The Th/U ratio for the Eastern Ghats is on average in the 20's (Barker, 2010). In the calcareous shale and the mud-rich shale there were Th/U ratios of 10-20. These values do not show any distinct signature for the Eastern Ghats. One GRS log in the silicate limestone yielded a Th value of 27.1 ppm, and a U value of 0.4 ppm. The Th/U ratio is 67.8. Another GRS log in the calcareous shale yielded U values of 0.2 ppm and Th values of 14.7 ppm which totals a Th/U ratio of 73. Due to the nature of the gamma ray spectrometer, I can assume that Th may be read by the gamma ray spectrometer instead of U and provide incorrect data. Due to the random nature of these values, it is unlikely that these values hold any confidence unless more data is acquired.

6.4 Petroleum Potential

The Kurnool Group goes through two stages of limestone deposition due to multiple transgression-regression events. These two unmetamorphosed limestones, Narji and Koilkuntla, may be a petroleum source. The Cuddapah Basin is grouped under Category IV by the Directorate General of Hydrocarbons, India, which means that it has a possible existence of hydrocarbons (Bastia, 2006). The Narji Limestone was the most well researched limestone in this study. The organic matter in the Narji has not been buried but remineralised in an environment. It is possible that this would be a rich gas reservoir if leakage has not taken place, although most Proterozoic basins are overmature and barren. Lying on top of the Narji Limestone is the Auk Shale, which could provide a potential seal for the reservoir. A potential trap could be the Panium Sandstone. If the Narji is deposited close to the Nallamali Fold Belt then there is a chance that there might be faulting or fracturing within the Panium which may cause a structural trap for the reservoir. Stratigraphic traps may also exist at the edges of the depositional area.

Although this may not be a conventional petroleum reservoir there is still the possibility that it could be used for in inventional shale gas. If the limestone is buried to a depth below ~1000m then there is a possibility that this could be used for petroleum resources. Further work should be completed to discover faults and fractures and confirm reservoir, seals and traps.

7. Conclusion

The main findings of this study are:

- The sediments from the Banaganapalle Formation and Panium Quartzite are sourced fromthe Dharwar Craton, based on U-Pb ages and Hf isotope data.
- Deposition of these sediments was in the Mesoproterozoic to the early Neoproterozoic, based on O and C stable isotopes.
- The sediments were deposited in a sub-tidal environment, ranging from a beach environment to a deep sub-tidal environment.
- There may be a chance of a petroleum reservoir due to the potential seal and trap formed by the sediments of the Kurnool Group.

8. Acknowledgements

First and foremost I thank my supervisors Alan Collins and Guillaume Backé, and my unofficial supervisor Galen Halverson, for assistance in the field and guiding me through the year in Adelaide - no matter where they were in the world. Thank you to the Geological Society of Australia for financial support and the Australian Government for supporting this work through an Australia India Strategic Research Fund Grant. In the field I was grateful for the help of Indian academics Sarbani Patranabis Deb and Dilip Saha, as well as the motivated Julie Mackintosh who, despite sickness, helped me a lot in the field. Thanks must go to Justin Payne for all his help this year from lab work to proof reading. Thanks must go to Grant Cox at L'Université du Québec à Montréal for doing the Carbon and Oxygen stable isotopes. I would also like to thank Adelaide Microscopy, especially Ben Wade and Angus Netting for all the early morning and late night assistance. I would like to thank Julie Mackintosh and Billy Reid for many discussions, as well as all of Honours 2010 for making it a very fun year. And last but not least I would like to thank my parents for their support emotionally and financially. They are always there to motivate me to do better. I would also like to thank Robert Barteletti for putting up with me when I was stressed and listening when I ranted

about my thesis, as well as family and friends any anyone else who asked how the thesis was going.

9. References

Anderson T., 2005. *Detrital zircons as tracers of sedimentary provenance: limiting conditions from startistics and numerical simulation.* Chemical Geology, **216**, 249-270.

Barker, A., 2010. *The thermal properties, temperature structure and thermal evolution of the Eastern Ghats, India.* Unpublished.

Bartley J. K., Semikhatov M. K., Kaufman A. J., Knoll A. H., Pope M. C., and Jacobsen S. B., 2000. *Global events across the Mesoporterozoic-Neoproterozoic boundary: C and Sr isotopic evidence from Siberia.* Precambrain Research **111**, 165-202.

Bastia R., 2006. *An overview of Indian sedimentary basins with special focus on emerging east coast deepwater frontiers.* The Leading Edge, 818-829.

Belousova E. A., Reid A. J., Griffin W. L., and O'Reilly S. Y., 2009. *Rejuvenation vs. Recycling of Archaean cryst in the Gawler Craton, South Australia: Evidence from U-Pb and Hf isotopes in detrital zircon.* Lithos, **113**, 570-582.

Chalapathi Rao N. V., Miller J. A., Pyle D. M., Madhavan V., 1995. *New Proterozoic K-Ar ages for some kimberlites and lamproites from the Cuddapah Basin and Dharwar Craton, South India: evidence for non-contemporaneous emplacement.* Precambrian Research **79**, 363-369.

Chakraborty P. P., Dey S., and Mohanty S. P. 2010. *Proterozoic platform sequences of Peninsular India: Implications towards basin evolution and supercontinent assembly.* Journal of Asian Earth Sciences, unpublished.

Chatterjee N. and Bhattacharji S. 2001. *Petrology, geochemistry and tectonic settings of the mafic dikes and sills associated with the evolution of the Proterozoic Cuddapah Basin of south India.* Proc. Indian Acad. Sci. **110**, 433-453.

Chaudhuri A. K., Mukhopadhyay J., Patranabis Deb S., Chanda S. K. 1999. *The Neoproterozoic Cratonic Successions of Peninsular India.* Gondwana Research **2**, no. 2, 213-225.

Chaudhuri A. K., Saha D., Deb G. K., Patranabis Deb S., Mukherjee M. K. and Ghosh G., 2002. *The Purana Basins of Southern Cratonic Provinve of India – A Case for Mesoproterozoic Fossil Rifts.* Gondwana Research **5**, 23-33.

Craig H. 1957. *Isotopic Standards For Carbon And Oxygen And Correction Factors For Mass-Spectrometric Analysis Of Carbon Dioxide*. Geochimica Et Cosmochimica Acta **12**, 133-149.

Crawford, A. & Compston, W. (1973). *The age of the Cuddapah and Kurnool systems, southern India.* Journal of the Geological Society of Australia, **19**, 453-464.

Dasgupta P. K., Biswas A., and Mukherjee R. 2005. *Cyclicity in Paleoproterozoic to Neoproterozoic Cuddapah Supergroup and its Significance in Basinal Evolution*.

Dobmeier C. J., and Raith M. M. 2003. *Crustal architecture and evolution of the Eastern Ghats Belt and adjacent regions of India.* Geological Society of London, Special Publications, **206,** 145-168.

Frank T. D., Kah L. C. and Lyons T. W., 2003. *Changes in organic matter production and accumulation mechanismfor isotopic evolution in the Mesoporterozoic.* Geol. Mag. **140**, 397-420.

Griffin W. L., Pearson N. J., Belousova E., Jackson S. E., Van Achterbergh E., O'Reilly S. Y. & Shee S. R. 2000. *The Hf isotope composition of cratonic mantle: LAM-MC-ICPMS analysis of zircon megacrysts in kimberlites*. Geochimica Et Cosmochimica Acta **64**, 133-147.

Griffin W. L., Powell W. J., Pearson N. J. & O'Reilly S. Y. (Editors) 2008. *GLITTER: Data Reduction Software for Laser Ablation ICP-MS. (Laser Ablation ICP-MS in the Earth Science: Current Practices and Outstanding Issues)*. Mineralogical Association of Canada, Ottowa.

Gupta A., 1997. *Primordial Storms: An Overview of Depositional Environment in Mid-Late Proterozoic Platforms of India.* Gondwana Research **1**, 291-298.

Halverson G. P., Maloof A. C., Schrag D. P., Dudás F. Ö. and Hurtgen, M., 2006. *Stratigraphy and geochemistry of a ca 800 Ma negative carcon isotope interval in northeastern Svalbard.* Chemical Geology, **237**, 23-45.

Howard K. E., Hand M., Barovich K. M., Reid A., Wade B. P. and Belousova E. A., 2009. *Detrital zircon ages: Improving interpretation via Nd and Hf isotopic data.* Chemical Geology **262**, 277-292.

Jackson S. E., Pearson N. J., Griffin W. L. And Belousova E. A. 2004. *The application of laser ablation-inductively coupled plasma-mass spectrometry to in-situ u-Pb zircon geochronology.* Chemical Geology **211** (1-2), 47-69.

Jayananda M., Moyen J. –F., Martin H., Peucat J. –J., Auvray B., and Mahabaleswar B., 2000. *Late Archean (2550 – 2520 Ma) juvenile magmatism in the Eastern Dharwar craton, southern India: constrains from geochronology, Nd-Sr isotopes and whole rock geochemistry.* Precambrian Research **99**, 225-254.

Kah L. A., Sherman A. G., Narbonne G. M., Knoll A. H. And Kaufman A. J., 1998. *$\delta^{13}C$ stratigraphy of the Proterozoic Bylot Supergroup, Baffin Island, Canada: implications for regional lithostratigraphic correlations.* Canadian Journal of Earth Science **36,** 313-332.

Kailasam, L.N. 1976. *Geophysical studies of the major sedimentary basins of the Indian craton, their deep structural features and evolution*. In: M.H.P. Bott (editor), Sedimentary Basins of Continental Margins and Cratons. Tectonophysics, **36** (l-3): 225-245

Kumar A., Bhaskar Rao Y. J., Sivaraman T. V., and Gopalan K 1996. *Sm-Nd ages of Archean metavolcanics of the Dharwar Craton, South India.* Precambrian Research **80**, 205-216.

Ludwig K. R., 2000. *Decay constant errors in U-Pb Concordia-intercept ages.* Chemical Geology, **166**, 315-318.

Madhava Rao D. and Gokhale K. V. G. K., 1973. *Ripple marks in quartzites from Kurnool Supergroup, Cuddapah Basin, India.* Journal of Sedimentary Petrology **43** 1122-1124.

Mackintosh J. N., 2010. *Age and basin Evolution of the Cuddapah Basin, India.* Unpublished.

Meen J. K., Rogers J. J. W., and Fullagar P. D., 1992. *Lead isotopic compositions of the Western Dharwar Craton, southern India: Evidence for distinct Middle Archean terranes in a Late Archean craton.* Geochimrca ei Cosmockimico Acla, **56**, 2455-2470.

Meert J. G., Pandit M. K., Pradhan V. R., Banks J., Sirianni R., Stroud M., Newstead B., and Gifford J. 2010. *Precambrian crustal evolution of Peninsular India: A 3.0 billion year odyssey.* Journal of Asian Earth Sciences, unpublished.

Meijerink A.M.J, Rao D.P, and Rupke J. 1985. *Stratigraphic and structural development of the Precambrian Cuddapah basin, S.E. India.* Precambrian Research, **26**, 57-97.

Mukhopadhyay D. and Basak K., 2009. *The Eastern Ghats Belt...A Polycyclic Granulite Terrain.* Journal Geological Society of India, **73**, 489-518.

Murthy, Y. G. K. 1978. *Salient features of the revised geological map of the Cuddapah basin.* 3rd Workshop on Status, Problems and Programmes in Indian Peninsular Shield. Institute of Indian Peninsular Geology, Hyderabad, 1-21.

Naganjaneyulu K. and Harinarayana, T. 2004. *Deep Crustal Electrical Signatres of Eastern Dharwar Craton, India.* Gondwana Research **7**, 951-960.

Pandey B.K., Gupta J.N., Sarma K.J., Sastry C.A. 1997. *Sm-Nd, Pb-Pb and Rb-Sr geochronology and petrogenesis of the mafic dyke swarm of Mahbubnagar, South India: implications for Paleoproterozoic crustal evolution of the Eastern Dharwar Craton*. Precambrian Research **84** 181 – 196

Peucat J. J., Mahabaleswar B. And Jayananda M., 1993. *Age of younger tonalitic magmatism and granulitic metamorphism in the South Indian transition zone (Krishnagiri area); comparison with older Peninsular gneisses from the Gorur-Hassan area.* Journal of Metamorphic Geology, **11**, 879-888.

Payne J. L., Barovich K. M., and Hand M., 2006. *Provenance of metasedimentary rocks in the nornthern Gawler Craton, Australia: Implications for Palaeoproterozoic reconstructions.* Precambrian Research, **148**, 275-291.

Raase, P., Raith, M., Ackermand, D. and Lal, R.K., 1986. *Progressive metamorphism of mafic rocks from greenschist to granulite facies in the Dharwar craton of south India*. J Geol., **94**, 261-282.

Radhakrishna B. P. And Naqvi S. M., 1986. *Precambrian Continental Crust and Its Evolution.* The Journal of Geology, **94**, 145-166.

Raman P.K., Murty, V.N., 1997. *Geology of Andhra Pradesh*. Geological Society of India, Bangalore.

Rickers K., Mezger K. and Raith M. M. 2001. *Evolution of the Continental Crust in the Proterozoic eastern Ghats Belt, India and new constrains for Rodinia reconstruction: implications from Sm-Nd, Rb-Sr and Pb-Pb isotopes*. Precambrian Research, **112**, 183-210.

Rogers J. J. W. 1986. *The Dharwar Craton and the Assembly of Peninsular India*. The Journal of Geology, **94**, 129-143.

Segal I., Halicz L. & Platzner I. T. 2003. *Accurate isotope ratio measurements of ytterbium by multiple collection inductively coupled plasma mass spectrometry applying erbium and hafnium in an improved double external normalization procedure.* Journal of Analytical Atomic Spectrometry **18**, 1217-1223.

Sharma M. And Shulka M., 1999. *Carbonaceous mega remains from the Neoproterozoic Owk Shale Fomration of the Kurnool Group, Andhra Pradesh, India.* Current Science, **79**, 1247-1251.

Simmat R. And Raith M. M., 2007. *U-Th-Pb monazite geochronometry of the Eastern Ghats Belt, India: Timing and spatial disposition of poly-metamorphism.* Precambrian Research, **162**, 16-39.

Singh A. P. And Mishra D. C. 2001. *Tectonosedimentary evolution of Cuddapah basin and Eastern Ghats mobile belt (India) as Proterozoic collision: gravity, seismic and geodynamic constraints*. Journal of Geodynamics **33**, 249-267.

Sláma J., Kosler J., Condon D. J., Crowley J. L., Gerdes A., Hanchar J. M., Horstwood M. S. A., Morris G. A., Nasdala L., Norberg N., Schaltegger U., Schoene B., Tubrett M. N. &

Whitehouse M. J. 2008. *Plešovice zircon -- A new natural reference material for U-Pb and Hf isotopic microanalysis.* Chemical Geology **249**, 1-35.

Taylor, P.N., Chadwick, B., Moorbath, S., Ramakrishnan, M. and Viswanathal, M.N., 1984. *Petrography, chemistry and isotopic ages of Peninsular gneiss, Dharwar acid volcanic rocks and the Chitradurga granite with special reference to the late Archaean evolution of the Karnataka craton, Southern India*. Precambrian Res., **23**, 349-375.

Upadhay D., Gerdes A. And Raith M. M. 2009. *Unravelling Sedeimentary Provenanse and Tectonothermal History of High Temperature Metapelies, Using Zircon and Monazite Chemistry: A Case Study from the Eastern Ghats Belt, India.* Journal of Geology, **117**, 665-683.

Vasudevan, D., Kröner, A.,Wendt, I.,Tobschall, H., in press. *Geochemistry, petrogenesis and age of felsic to intermediate metavolcanic rocks from the Palaeoproterozoic Nellore Schist Belt, Vinjamur, Andhra Pradesh, India, J*. Asian Earth Sciences.

Veevers J. J., Saeed A., Belousova E. A., and Griffin W. L., 2004. *U-Pb ages and source composition by Hf-isotope and trace-element analysis of detrital zircons in Permian sandstone and modern sand from southwestern Australia and a review of the paleogeographical and denudational history of the Yilgarn Craton*. Earth Science Reviews, **68**, 245-279.

Vervoort, J. D., Patchett P. J., Söderlund U., and M. Baker 2004. *Isotopic composition of Yb and the determination of Lu concentrations and Lu/Hf ratios by isotope dilution using MC-ICPMS,* Geochem. Geophys. Geosyst., **5**, Q11002, doi:10.1029/2004GC000721.

Zachariah J. K., Bhaskar Rao Y. J., Srinivasan R., Gopalan K., 1999. *Pb, Sr and Nd isotope systematic of uranium mineralised stromatolitic dolomites from the Proterozoic Cuddapah Supergroup, south India: constrains on age and provenance.* Chemical Geology **162**, 49-64.

10. Figure Captions

Figure 1. Simple map fo India, showing the relationship between the Cuddpah Basin, Eastern Ghats and the Dharwar Craton.

Figure 2. Map of the Cuddpah Basin showing the main basin and the two sub-bains. The light grey dots indicate the location areas.

Figure 3. Photographs of facies characteristics in the Kurnool Group; **A)** isolated clatsts, **B)** fine and course grains, **C)** trough cross bedding, **D)** cross bedding, **E)** intraclasts insilicate limestone, **F)** ribbons, **G)** hummocky cross stratification, **H)** clay beds in silicate limestone, **I)** grainstone, **J)** maximum flooding surface suspension bedding, **K)** massive sandstone and **L)** characteristic mud-rich shale.

Figure 4. Key for sedimentary logs showing the type of facies and sedimentary structures.

Figure 5. Stratigraphic log of Narji 1 shows the tranision between Banaganapalle Formation and the Narji Limestone, at the bottom of the Kurnool Group. The key for the sedimentary structures and facies is given in Figure 4. Facies descriptions are given in text. GRS data is shown in Total, K, U and Th and this significance of this is discussed in text. There were no samples taken throughthis section.

Figure 6. Stratigraphic log of Narji 2 shows the transition between the Narji, Auk and Panium Formations in the middle of the Kurnool Group. The key for the sedimentary structures and facies is given in Figure 4. Facies descriptions are given in text. GRS data is shown in Total, K, U and Th and this significance of this is discussed in text. $\delta^{13}C_{carb}$ and $\delta^{18}O_{carb}$ values are plotted in ‰ relative to VPDB (Table 6.), where VPDB is 0‰. The sample for CU10-22 was sampled in this log.

Figure 7. Stratigraphic log of Auk. This shows the relationship between Auk Shale and Panium Quartzite, in the middle of the Kurnool Group. The key for the sedimentary structures and facies is given in Figure 4. Facies descriptions are given in text. GRS data is shown in Total, K, U and Th and this significance of this is discussed in text.

Figure 8. Graphs of data from CU10-05, CU10-06, CU10-22. **a)** A concordia plot of the LA-ICPMS U-Pb data of zircons in the lower Banaganapalle Formation (CU10-05). The smaller box shows the Concordia diagram only with 100 ± 10% concordancy. **b)** Probability density distribution diagram showing ^{207}Pb/ ^{206}Pb for sample CU10-05, which is from the Banaganapalle Formation, and it shows that there is a range of possible sources. **c)** A concordia plot of the LA-ICPMS U-Pb data of zircons in the lower Banaganapalle Formation (CU10-06). The smaller box shows the Concordia diagram only with 100 ± 10% concordancy. **d)** Probability density distribution diagram showing ^{207}Pb/ ^{206}Pb for sample CU10-06, which is also from the Banaganapalle Formation, and it shows that there are two main groups of data which may relate to difference provenances. **e)** A concordia plot of the LA-ICPMS U-Pb data of zircons in the lower Panium Quartzite (CU10-22). The smaller box shows the Concordia diagram only with 100 ± 10% concordancy. **f)** Probability density distribution diagram showing ^{207}Pb/ ^{206}Pb for sample CU10-22, which is from the Panium Quartzite, and it shows that there is one main group of data.

Figure 9. This graph represents inital U-Pb detrital zircon ages for the LA-ICPMS plotted against the ε_{Hf}^{T} and shows where the zircons lie relative to CHUR and depleted mantle (DM).

Figure 10. This shows initial U-Pb detrital zircon ages for the LA-ICPMS plotted against ^{176}Hf/^{177}Hf initial to display the crustal growth lines for average continental crustal ^{176}Lu/^{177}Hf values of 0.0015.

Figure 11. Stable isotope plor for Narji 2 where the $\delta^{13}C_{carb}$ and $\delta^{18}O_{carb}$ values are plotted in ‰ relative to VPDB (Table 6.), where VPDB is 0‰.

Figure 12. Stable isotope plot for Narji 3 where the $\delta^{13}C_{carb}$ and $\delta^{18}O_{carb}$ values are plotted in ‰ relative to VPDB (Table 6.), where VPDB is 0‰.

Figure 13. Stable isotope plots for both Narji 2 and Narji 3 sections showing the correlation between the two. The two plots show the same trends.

Figure 14. Crossplot of $\delta^{13}C_{carb}$ against $\delta^{18}O_{carb}$ for all carbonate samples from the Narji Formation. Values are plotted in ‰ relative to VPDB (Table 6.), where VPDB is 0 ‰.

11. List of Tables

12. Figures

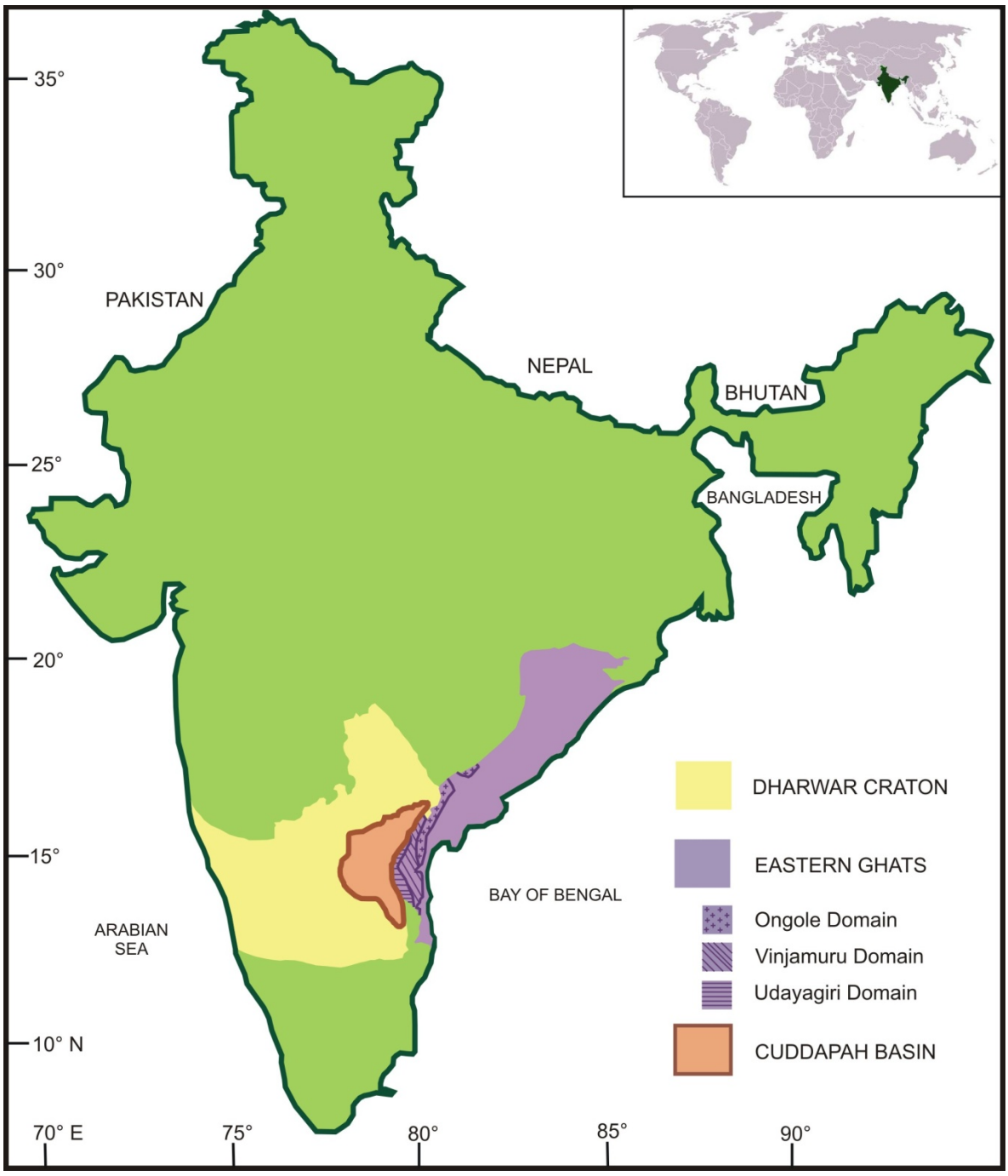

Figure 1.

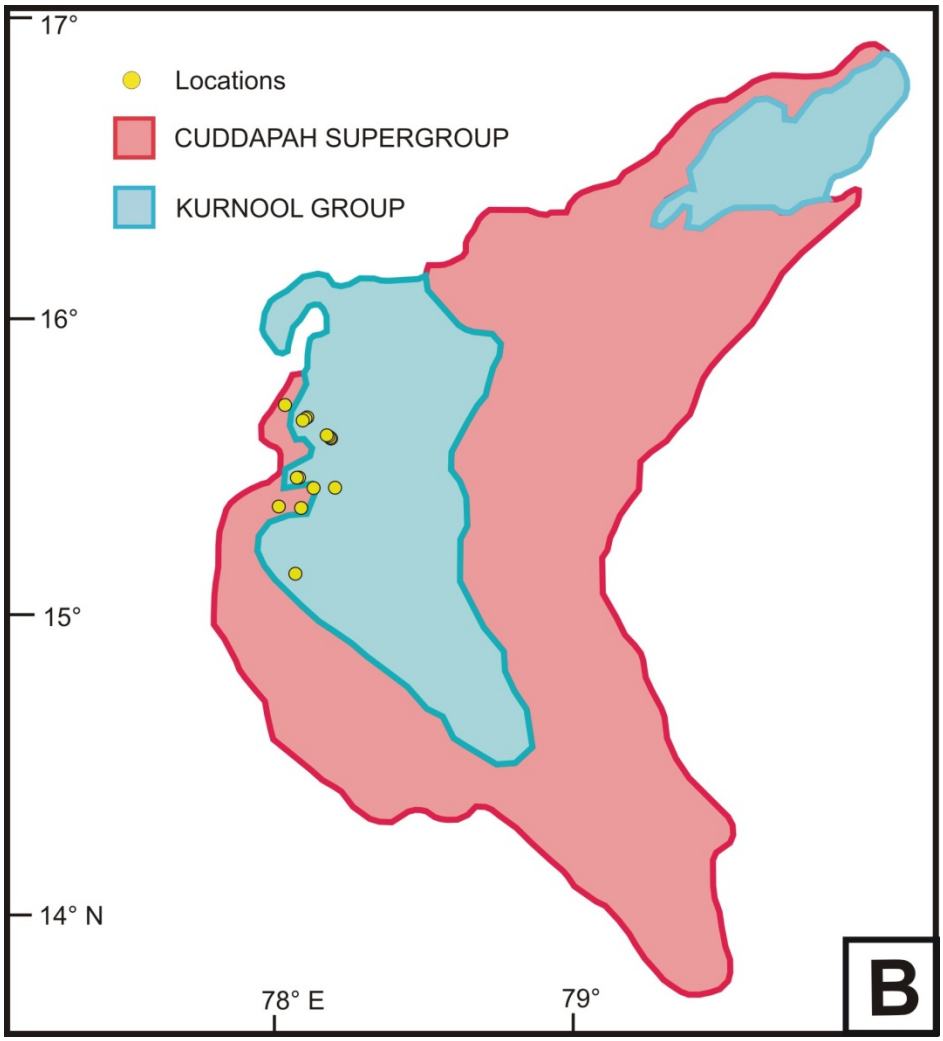
17°
Locations
CUDDAPAH SUPERGROUP
KURNOOL GROUP
16°
15°
14° N
78° E
79°
B

Figure 2.

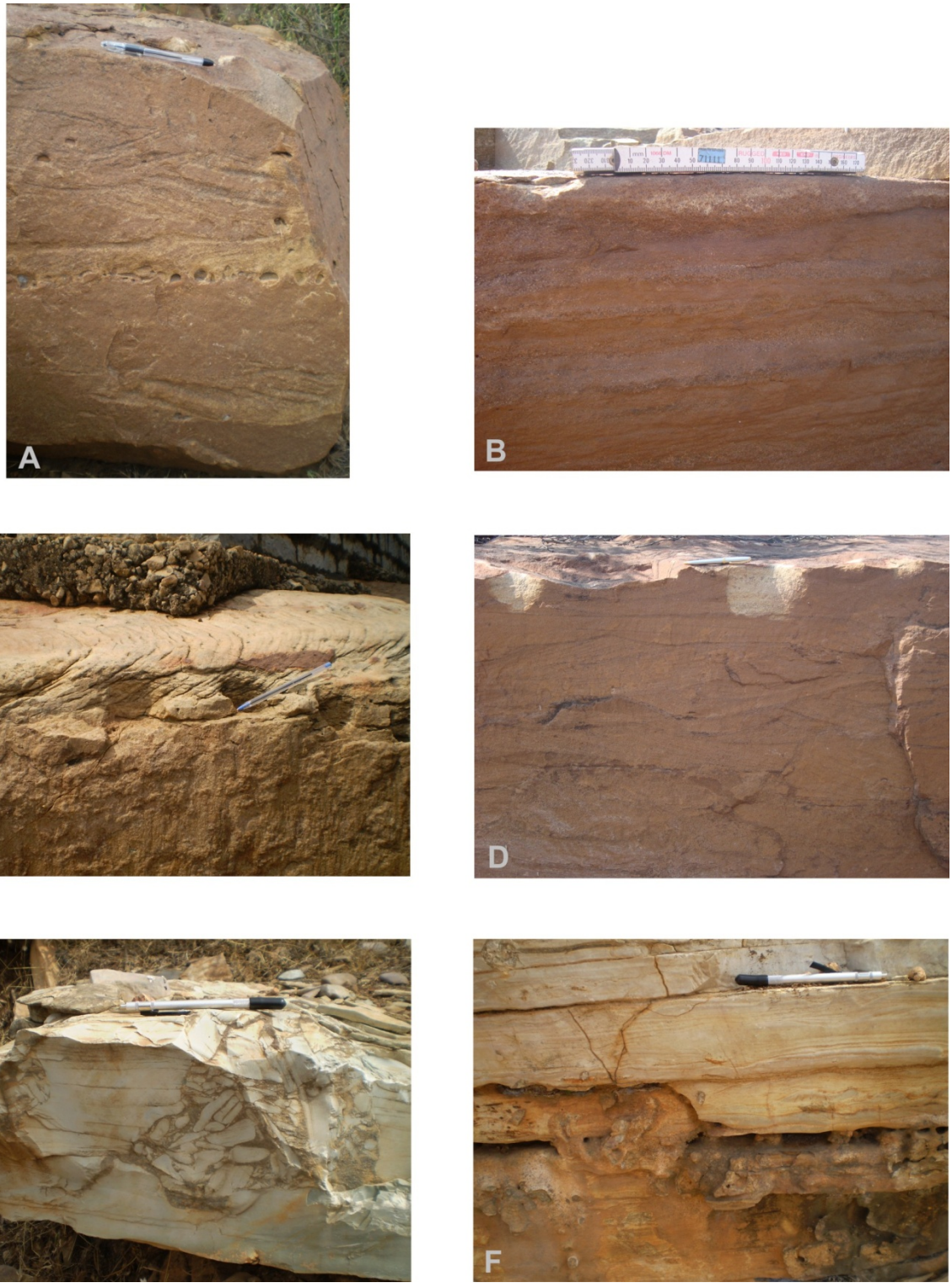

Figure 3 – A to F

Figure 3 – G to L

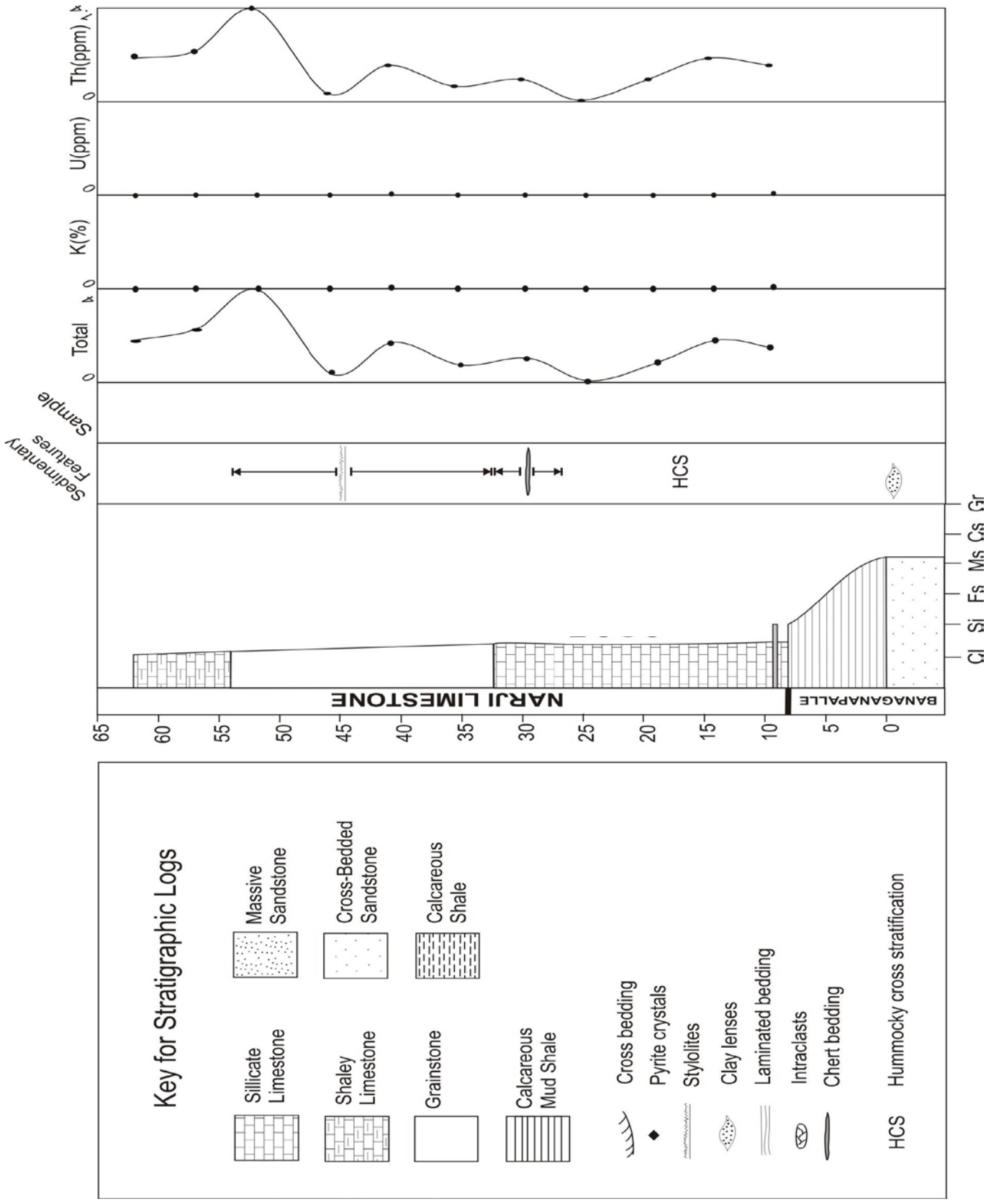

Figures 4 and 5.

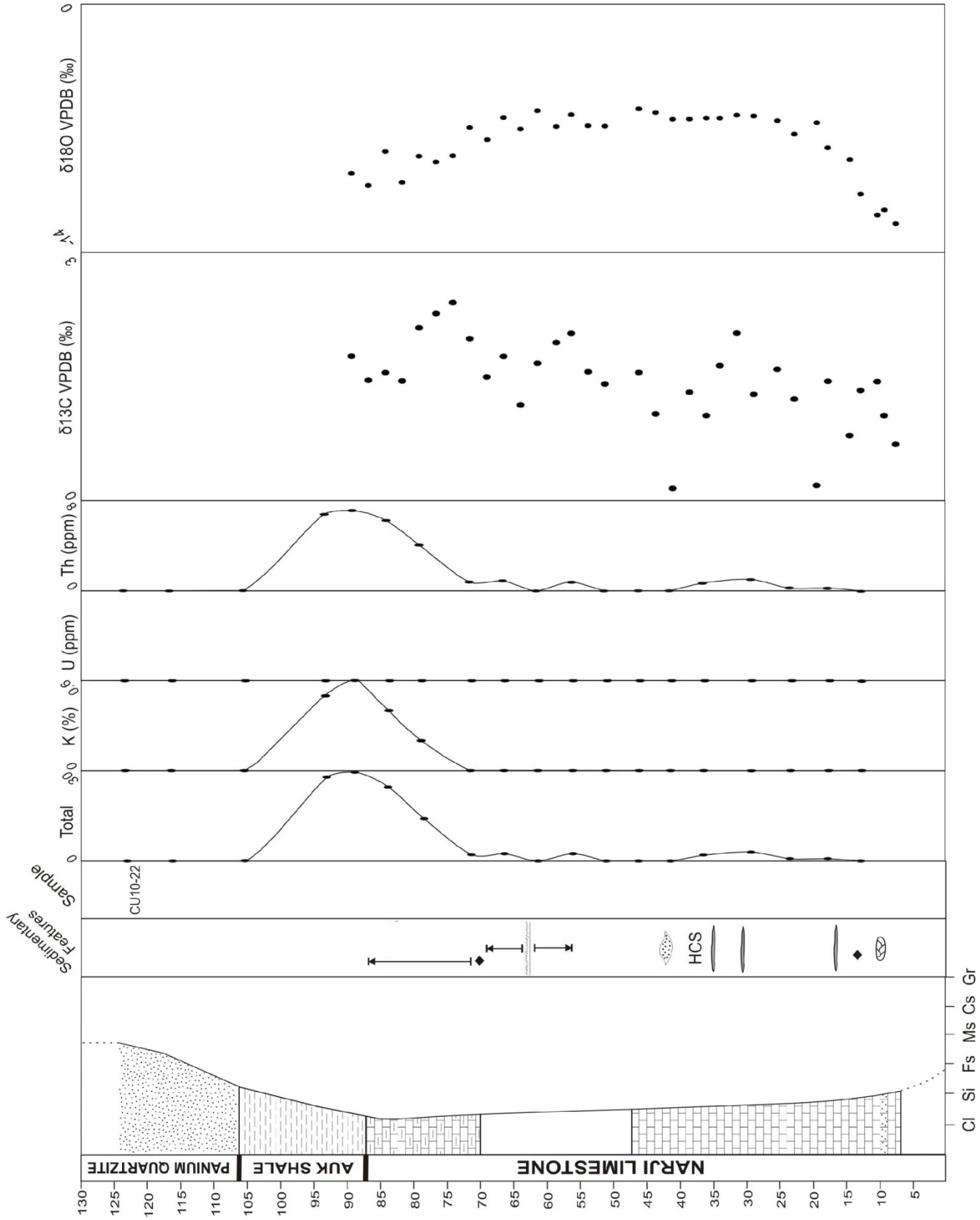
δ18O VPDB (‰)
δ13C VPDB (‰)
Th (ppm)
U (ppm)
K (%)
Total
Sample
CU10-22
Sedimentary Features
HCS
Cl Si Fs Ms Cs Gr
PANIUM QUARTZITE
AUK SHALE
NARJI LIMESTONE
130 125 120 115 110 105 100 95 90 85 80 75 70 65 60 55 50 45 40 35 30 25 20 15 10 5

Figure 6.

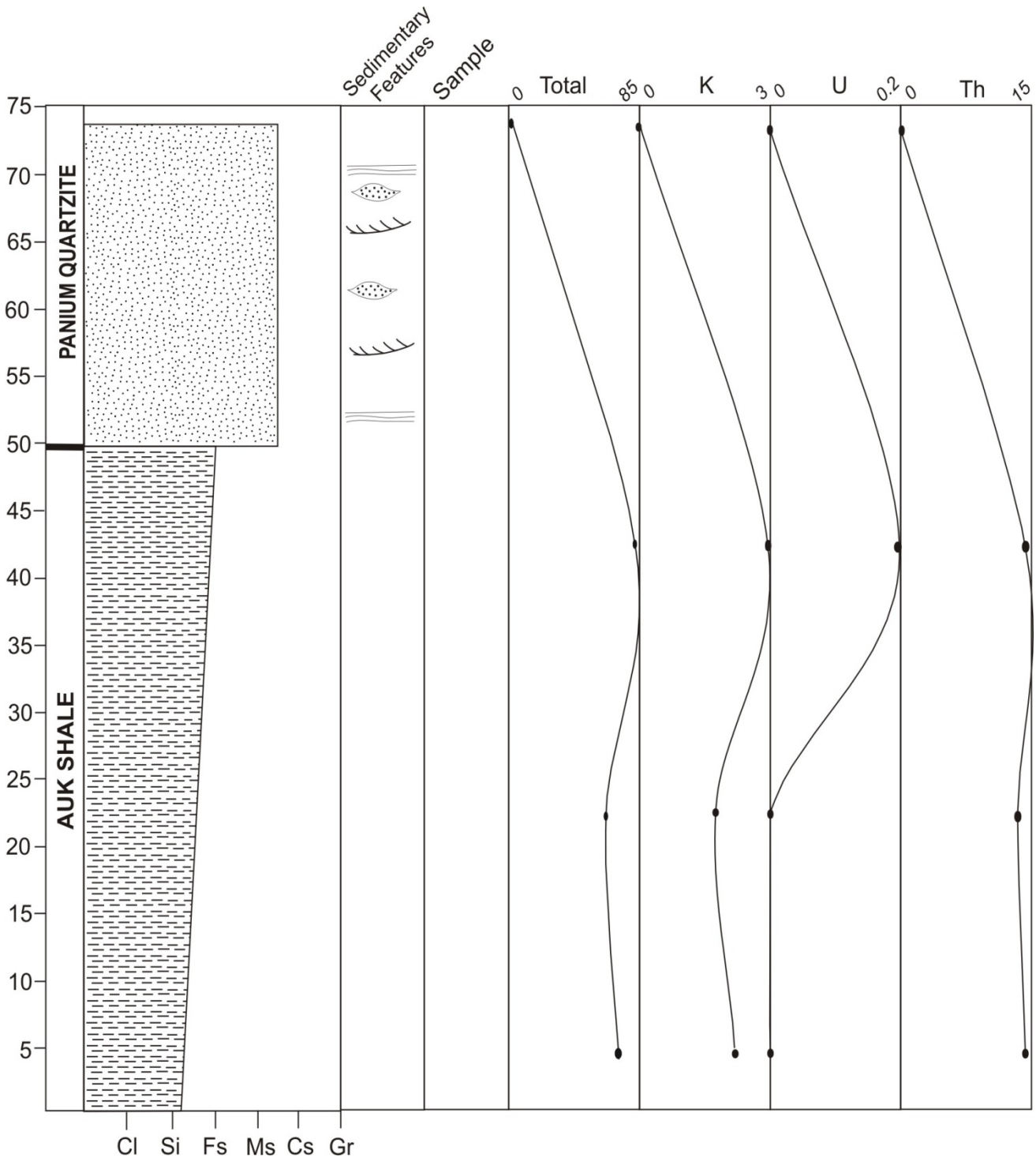
Sedimentary Features
Sample
0 Total 85
0 K 3
0 U 0.2
0 Th 15
75
70
65
60
55
50
45
40
35
30
25
20
15
10
5
PANIUM QUARTZITE
AUK SHALE
Cl Si Fs Ms Cs Gr

Figure 7

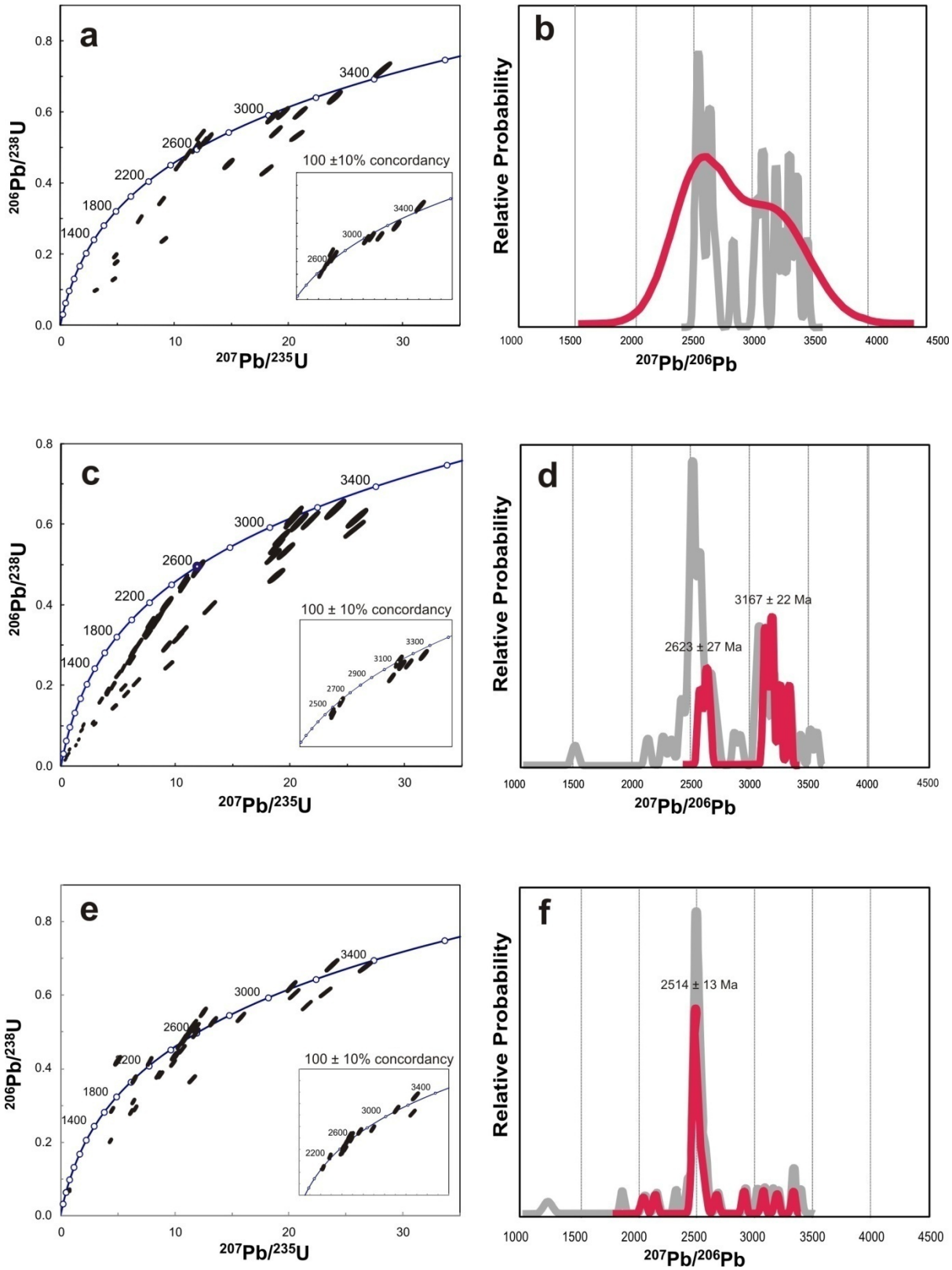
a
b
c
d
e
f
$^{206}Pb/^{238}U$
$^{207}Pb/^{235}U$
$^{207}Pb/^{206}Pb$
Relative Probability
100 ±10% concordancy
100 ± 10% concordancy
3167 ± 22 Ma
2623 ± 27 Ma
2514 ± 13 Ma

Figure 8.

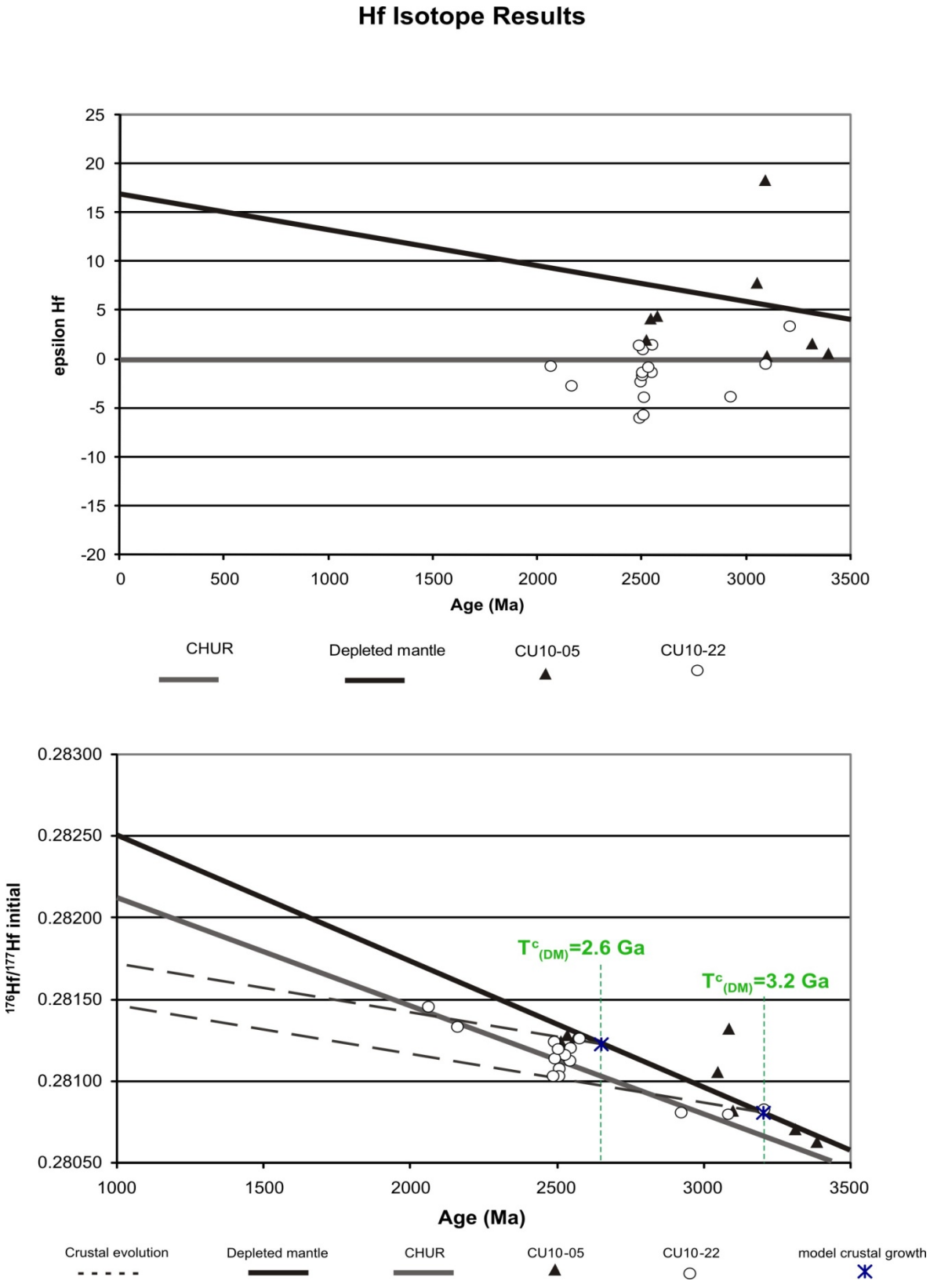

Figures 9 and 10.

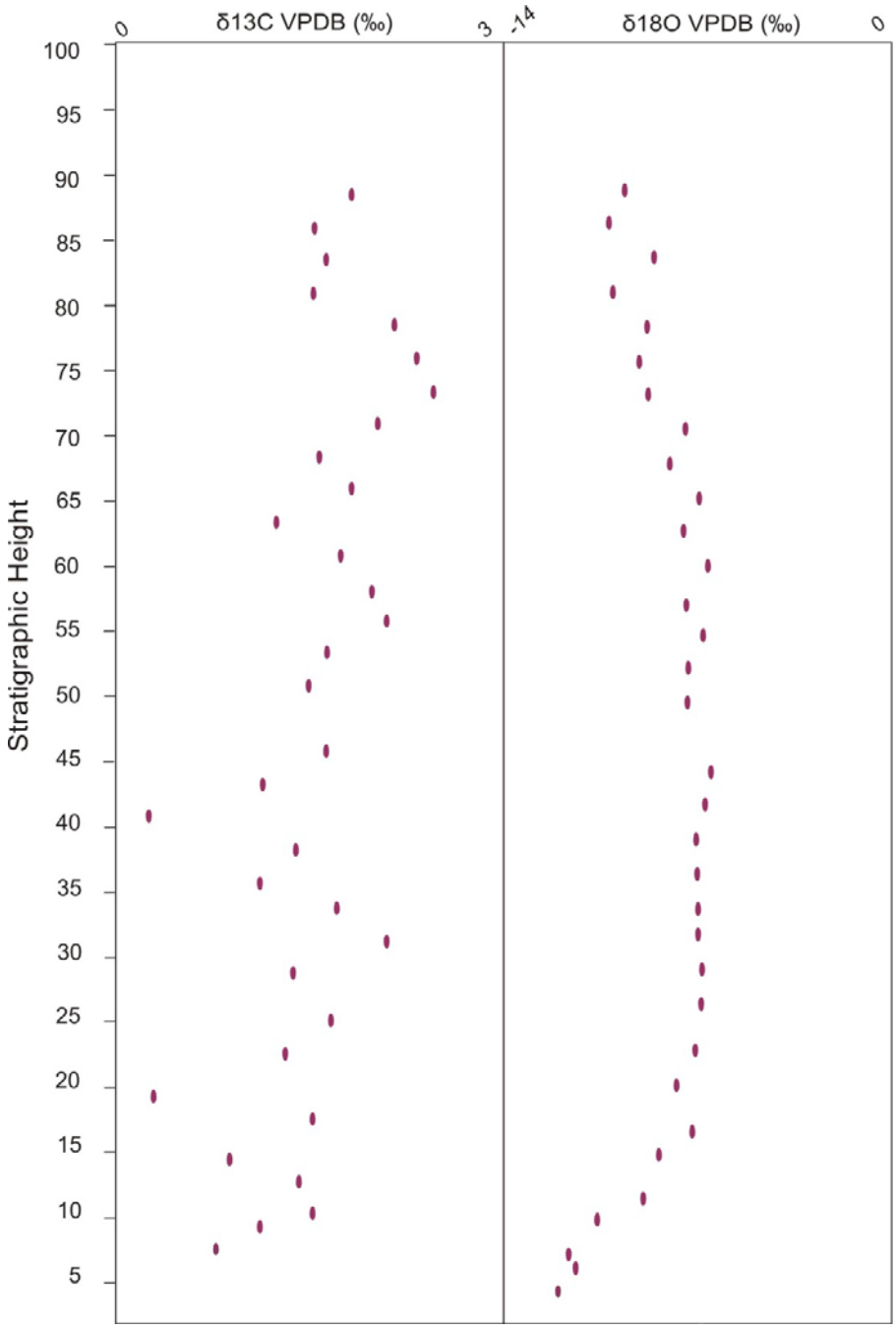
δ13C VPDB (‰)
δ18O VPDB (‰)
Stratigraphic Height
0
3
-14
0
100
95
90
85
80
75
70
65
60
55
50
45
40
35
30
25
20
15
10
5

Figure 11.

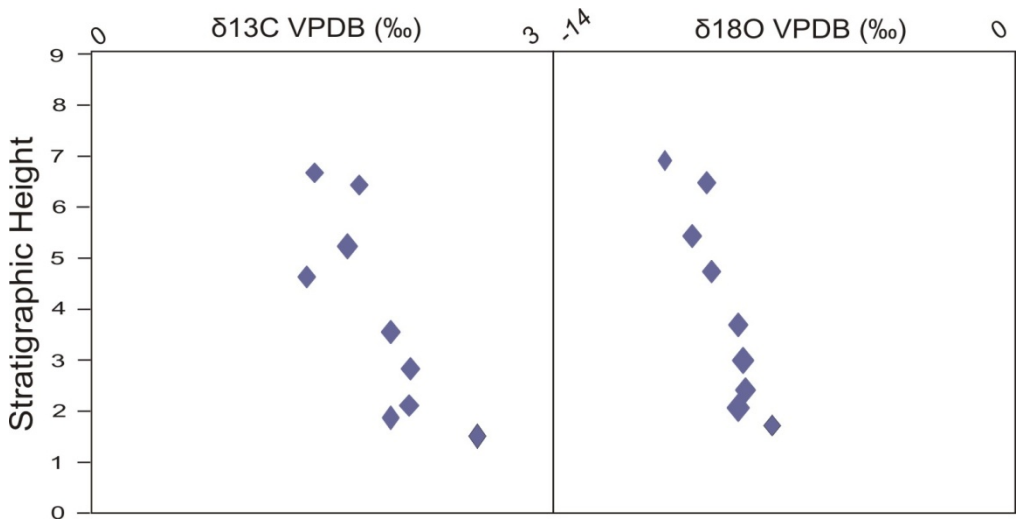
δ13C VPDB (‰)
δ18O VPDB (‰)
Stratigraphic Height
0
3
-14
0
9
8
7
6
5
4
3
2
1
0

Figure 12.

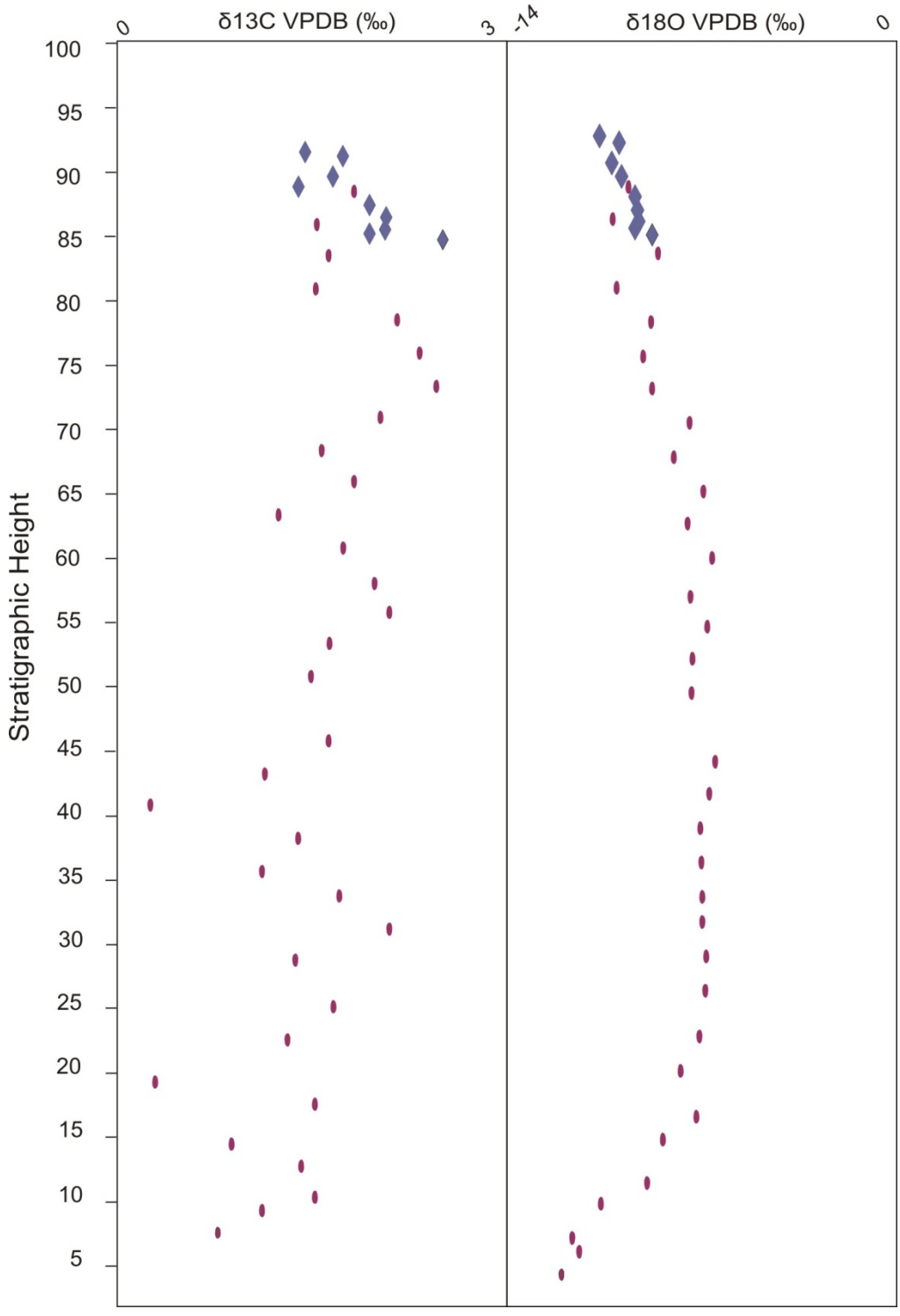
δ13C VPDB (‰)
δ18O VPDB (‰)
Stratigraphic Height
100
95
90
85
80
75
70
65
60
55
50
45
40
35
30
25
20
15
10
5

Figure 13.

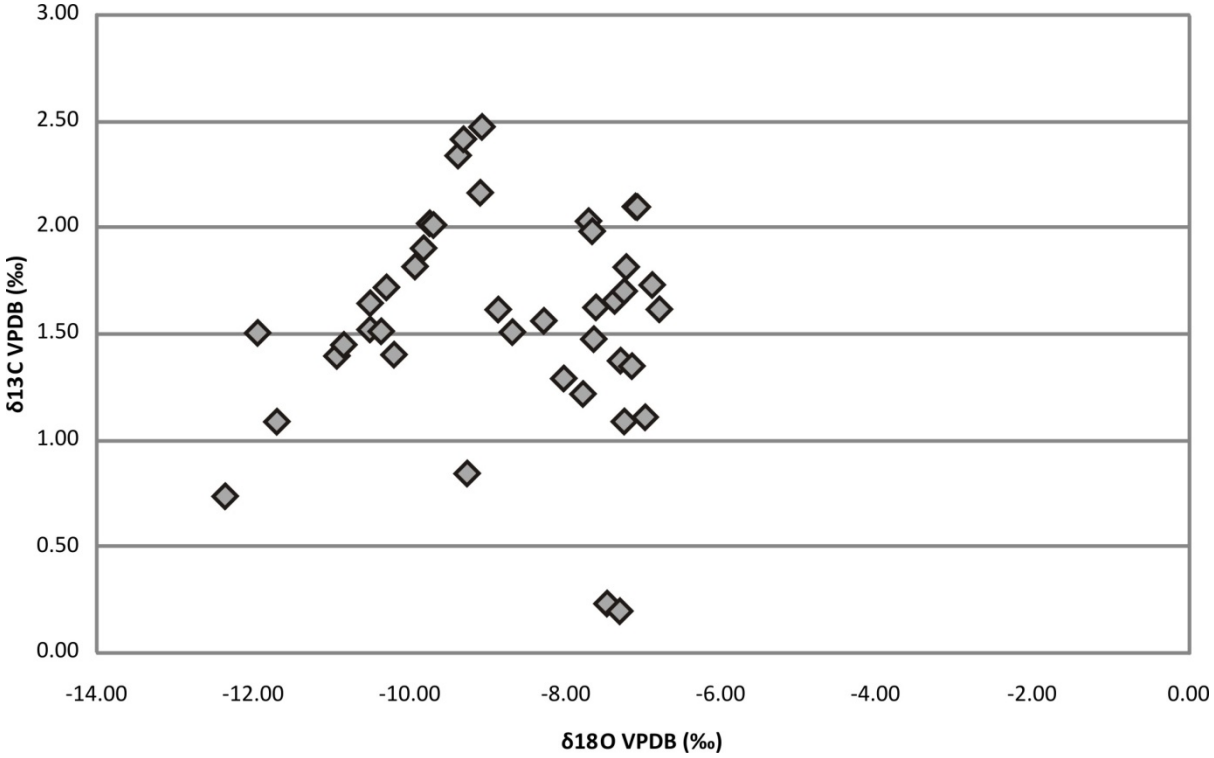
3.00
2.50
2.00
1.50
1.00
0.50
0.00
δ13C VPDB (‰)
-14.00
-12.00
-10.00
-8.00
-6.00
-4.00
-2.00
0.00
δ18O VPDB (‰)

Figure 14.

14. Tables

Table 1.

Group	Formation	Dominant Lithology
Kurnool Group	Nandyal Shale	Calcareous shale
	Koilkuntla Limestone	Limestone, conglomerate, quarzite and shale
	Panium Quartzite	Massive sandstone
	Auk Shale	Shale with thin sandy interbeds
	Narji Limestone	Well bedded limestone with pyrite
	Banaganapalle Formation	Diamondiferous comglomerate and sandstone
	~ ~ ~ ~ ~ unconformity ~ ~ ~ ~ ~	
Nallamali Group	Cumbum Formation	Shale

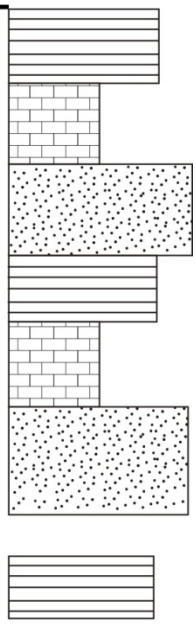

Table 2.

Section	Formations	Location		Total length (m)
		Latitude (N)	Longitude (E)	
Narji 1	Banaganapalle and Narji	15° 32' 49.7"	78° 17' 48.9"	65.5
Narji 2	Narji, Auk and Panium	15° 25' 23.4"	78° 09' 50.1"	124.4
Auk	Auk and Panium	15° 06' 50.3"	78° 06' 55.6"	73.6

Table 3.

Formation	Cross Bedding?	Type of Ripple	Dip	Dip Dirn.
Banaganapalle	x	-	31	58
	x	-	18	177
		symmetrical	0	105 / 285
		symmetrical	3	89 / 269
		symmetrical	3	78 / 258
		symmetrical	1	64 / 244
		symmetrical	1	67 / 247
		symmetrical	3	63 / 243
		symmetrical	3	63 / 234
		symmetrical	1	75 / 255
		symmetrical	0	83 / 263
		symmetrical	0	82 / 262
		symmetrical	5	82 / 262
		symmetrical	2	90 / 270

Table 4.

Formation	Strat Log	#	Total	K (%)	U (ppm)	Th (ppm)	Th/U (ppm)
Cross Bedded Sandstone		34	9.7	0.5	0	0.6	
Cross Bedded Sandstone		35	13.4	0.7	0	0.9	
Cross Bedded Sandstone		36	8.1	0.5	0	0	
Cross Bedded Sandstone		37	0	0	0	0	
Cross Bedded Sandstone		39	4.9	0.3	0	0.2	
Cross Bedded Sandstone		40	10.1	0.7	0	0	
Calcareous Mud Shale		41	4.7	0.3	0	0	
Cross Bedded Sandstone		42	13.5	0.9	0	0	
Cross Bedded Sandstone		43	24.7	1.6	0	0.4	
Sillicate Limestone		44	6.6	0	0	2.2	
Sillicate Limestone		45	0.8	0	0	0.3	
Grainstone		46	0.9	0	0	0.3	
Massive Sandstone		49	0	0	0	0	
Sillicate Limestone	Narji 2	88	15.8	0.3	0	3.7	
Sillicate Limestone	Narji 2	89	1.9	0	0	0.6	
Sillicate Limestone	Narji 2	90	3.8	0	0	1.2	
Sillicate Limestone	Narji 2	91	0	0	0	0	
Sillicate Limestone	Narji 2	92	0.7	0	0	0.2	
Sillicate Limestone	Narji 2	93	0.7	0	0	0.2	
Sillicate Limestone	Narji 2	94	2.8	0	0	0.9	
Sillicate Limestone	Narji 2	95	1.8	0	0	0.6	
Grainstone	Narji 2	96	0	0	0	0	
Grainstone	Narji 2	97	0	0	0	0	
Grainstone	Narji 2	98	2.3	0	0	0.7	
Grainstone	Narji 2	99	0	0	0	0	
Grainstone	Narji 2	100	2.3	0	0	0.8	
Shaley Limestone	Narji 2	101	2	0	0	0.7	
Shaley Limestone	Narji 2	102	14.2	0.2	0	3.7	
Shaley Limestone	Narji 2	103	23.7	0.4	0	5.7	
Shaley Limestone	Narji 2	104	28.5	0.6	0	6.5	
Calcarous Shale	Narji 2	105	26.9	0.5	0	6.2	
Massive Sandstone	Narji 2	106	0	0	0	0	
Massive Sandstone	Narji 2	107	0	0	0	0	
Massive Sandstone	Narji 2	108	0	0	0	0	
Calcarous Shale		109	82.4	1.5	1.6	16.3	10.2
Calcarous Shale		110	76.6	1.2	1	17	17.0
Mud-Rich Shale		135	90.1	2	1.6	16.6	10.4
Mud-Rich Shale		136	85.4	2.1	0	17.6	
Mud-Rich Shale		137	81.4	1.7	0.8	16.7	20.9
Cross Bedded Sandstone		138	8.1	0.5	0	0.5	
Sillicate Limestone	Narji 1	139	177	6.1	0.4	27.1	67.8
Sillicate Limestone	Narji 1	140	67.8	2.3	0	10.8	
Sillicate Limestone	Narji 1	141	1.4	0	0	0.5	
Sillicate Limestone	Narji 1	142	1.8	0	0	0.6	
Sillicate Limestone	Narji 1	143	0.8	0	0	0.3	
Sillicate Limestone	Narji 1	144	0	0	0	0	

Formation	Strat Log	#	Total	K	U	Th	
Sillicate Limestone	Narji 1	145	1	0	0	0.3	
Sillicate Limestone	Narji 1	146	0.7	0	0	0.2	
Sillicate Limestone	Narji 1	147	1.7	0	0	0.5	
Grainstone	Narji 1	148	0.3	0	0	0.1	
Grainstone	Narji 1	149	4	0	0	1.3	
Shaley Limestone	Narji 1	150	2.3	0	0	0.7	
Shaley Limestone	Narji 1	151	1.8	0	0	0.6	
Massive Sandstone		152	5.5	0	0	1.8	
Shaley Limestone		163	21.7	0.2	0	6	
Shaley Limestone		164	12.4	0	0	3.8	
Clay-Rich Limestone		165	30.9	0.5	0	7.5	
Clay-Rich Limestone		166	29.4	0.5	0	7	
Calcarous Shale	Auk	173	74.8	2	0	14.5	
Calcarous Shale	Auk	174	65.5	1.6	0	13.6	
Calcarous Shale	Auk	175	86.6	2.7	0.2	14.6	73
Massive Sandstone	Auk	176	0	0	0	0	
Cross Bedded Sandstone		184	5.8	0.4	0	0	

Table 5.

CU10-05	Isotope ratios								Ages (Ma)							
Spot name	Pb^{207}/Pb^{206}	± 1 s	Pb^{206}/U^{238}	± 1 s	Pb^{207}/U^{235}	± 1 s	Pb^{208}/Th^{232}	± 1 s	Rho	Pb^{207}/Pb^{206}	± 1 s	Pb^{206}/U^{238}	± 1 s	Pb^{207}/U^{235}	± 1 s	Pb^{208}/Th^{232}	± 1 s	Conc. (%)	Age
CU1005_22	0.16584	0.00186	0.53599	0.0089	12.25059	0.2041	0.13189	0.00269	0.997	2516.1	18.73	2766.6	37.3	2623.8	15.64	2504.1	48.04	110	2516
CU1005_18	0.1665	0.00196	0.45087	0.00769	10.34708	0.17593	0.08075	0.00138	0.997	2522.8	19.63	2399.1	34.2	2466.3	15.74	1569.5	25.85	95	2523
CU1005_13	0.1679	0.00182	0.48111	0.00786	11.13709	0.18049	0.06873	0.00108	0.992	2536.8	18.02	2532.1	34.2	2534.7	15.1	1343.6	20.45	100	2537
CU1005-8	0.16883	0.00187	0.29917	0.00474	6.96218	0.11056	0.06804	0.00104	0.998	2546.1	18.4	1687.2	23.5	2106.6	14.1	1330.4	19.68	66	2546
CU1005-9	0.17099	0.00192	0.5022	0.00832	11.84231	0.19538	0.11032	0.00155	0.996	2567.4	18.69	2623.2	35.7	2592	15.45	2115.2	28.14	102	2567
CU1005_12	0.17675	0.00213	0.51312	0.00867	12.51035	0.2126	0.1164	0.00179	0.994	2622.6	19.88	2669.9	37	2643.5	15.98	2225.6	32.33	102	2623
CU1005-3	0.17804	0.00206	0.19651	0.0031	4.82337	0.07765	0.02227	0.00035	0.980	2634.7	19.1	1156.6	16.7	1789	13.54	445.1	7	44	2635
CU1005_11	0.17818	0.00211	0.52622	0.00844	12.9213	0.21205	0.14696	0.00229	0.977	2636	19.54	2725.5	35.6	2673.9	15.47	2771.4	40.44	103	2636
CU1005-10	0.1832	0.00219	0.35046	0.00561	8.84692	0.14312	0.04421	0.00069	0.990	2682	19.61	1936.8	26.8	2322.3	14.76	874.4	13.31	72	2682
CU1005_20	0.20081	0.00211	0.17706	0.00305	4.89586	0.08073	0.01126	0.0002	0.957	2832.8	17.05	1050.9	16.7	1801.5	13.9	226.4	3.9	37	2833
CU1005_21	0.22591	0.0028	0.09916	0.00167	3.08863	0.0534	0.0218	0.00077	0.974	3023.3	19.72	609.5	9.82	1429.9	13.26	436	15.27	20	3023
CU1005_14	0.22941	0.00255	0.58608	0.0101	18.53012	0.30991	0.08724	0.00154	0.970	3047.9	17.67	2973.5	41.1	3017.7	16.11	1690.5	28.69	98	3048
CU1005_19	0.23491	0.00244	0.45501	0.00774	14.73639	0.24003	0.057	0.00103	0.958	3085.8	16.49	2417.5	34.3	2798.4	15.49	1120.5	19.78	78	3086
CU1005_17	0.23627	0.00248	0.59848	0.00988	19.49336	0.3145	0.10219	0.00147	0.977	3095	16.67	3023.7	39.8	3066.6	15.58	1966.7	26.88	98	3095
CU1005-2	0.25152	0.00263	0.54488	0.00883	18.8819	0.30137	0.0803	0.00126	0.985	3194.4	16.47	2803.9	36.9	3035.8	15.39	1561.2	23.55	88	3194
CU1005-5	0.25414	0.00263	0.59944	0.00925	20.99941	0.3171	0.15145	0.0022	0.979	3210.7	16.24	3027.6	37.3	3138.6	14.64	2850.4	38.57	94	3211
CU1005-1	0.2623	0.00262	0.12943	0.00201	4.68056	0.07111	0.0186	0.00023	0.978	3260.6	15.61	784.6	11.5	1763.8	12.71	372.5	4.59	24	3261
CU1005-4	0.27105	0.00282	0.64191	0.0107	23.97175	0.37947	0.09689	0.00119	0.950	3312.1	16.22	3196.5	42	3267.2	15.43	1869.3	22	97	3312
CU1005-7	0.27288	0.00286	0.24072	0.00399	9.05886	0.14639	0.02439	0.00035	0.975	3322.6	16.31	1390.4	20.7	2344	14.78	487.1	6.86	42	3323
CU1005-6	0.28158	0.00301	0.53317	0.00827	20.69603	0.31505	0.09357	0.00144	0.981	3371.7	16.59	2754.8	34.8	3124.5	14.74	1807.9	26.63	82	3372
CU1005_15	0.28477	0.00322	0.71825	0.01218	28.2076	0.46839	0.15559	0.00268	0.979	3389.3	17.5	3489.5	45.7	3426.3	16.28	2922.9	46.82	103	3389
CU1005_16	0.29992	0.0033	0.43552	0.00712	18.01222	0.29146	0.04786	0.00085	0.990	3469.8	16.95	2330.6	32	2990.4	15.57	944.9	16.34	67	3470

CU10-06	Isotope ratios									Ages (Ma)									
Spot name	Pb^{207}/Pb^{206}	± 1 s	Pb^{206}/U^{238}	± 1 s	Pb^{207}/U^{235}	± 1 s	Pb^{208}/Th^{232}	± 1 s	Rho	Pb^{207}/Pb^{206}	± 1 s	Pb^{206}/U^{238}	± 1 s	Pb^{207}/U^{235}	± 1 s	Pb^{208}/Th^{232}	± 1 s	Conc. (%)	Age
06_48	0.0913	0.00135	0.02829	0.00041	0.35464	0.00588	0.00587	0.00012	0.874	1452.7	27.81	179.9	2.6	308.2	4.41	118.2	2.36	12	1452.7
06_51	0.12885	0.00153	0.04153	0.00052	0.73799	0.0099	0.00821	0.00013	0.933	2082.3	20.68	262.3	3.24	561.2	5.78	165.2	2.64	13	2082.3
06_22	0.13908	0.00155	0.10264	0.00134	1.96794	0.02635	0.01218	0.00026	0.975	2215.7	19.21	629.9	7.82	1104.6	9.02	244.8	5.09	28	2215.7
06_53	0.14488	0.00183	0.09	0.0013	1.79794	0.02779	0.00805	0.00014	0.935	2286.3	21.62	555.6	7.66	1044.7	10.08	162	2.9	24	2286.3
06_11	0.15221	0.00165	0.1632	0.00229	3.42556	0.04782	0.02373	0.0003	0.995	2370.9	18.36	974.6	12.69	1510.3	10.97	474.1	6.01	41	2370.9
06_45	0.15243	0.00191	0.03164	0.00044	0.66473	0.00987	0.00634	0.00009	0.937	2373.3	21.23	200.8	2.78	517.5	6.02	127.7	1.88	8	2373.3
06_35	0.15533	0.00223	0.02681	0.00041	0.57359	0.00944	0.00284	0.00014	0.929	2405.5	24.22	170.5	2.58	460.3	6.09	57.3	2.77	7	2405.5
06_19	0.15823	0.00167	0.22887	0.00309	4.99343	0.0671	0.0305	0.00044	0.995	2436.9	17.81	1328.6	16.19	1818.2	11.37	607.3	8.57	55	2436.9
06_26	0.15827	0.0018	0.18717	0.00243	4.08272	0.05472	0.04147	0.00075	0.969	2437.3	19.17	1106	13.18	1650.9	10.93	821.3	14.61	45	2437.3
06_15	0.15879	0.0017	0.35607	0.00507	7.80162	0.10931	0.03651	0.00056	0.984	2442.8	17.97	1963.5	24.12	2208.4	12.61	724.8	11.01	80	2442.8
06_49	0.1608	0.0023	0.01628	0.00023	0.36059	0.00571	0.00727	0.00012	0.892	2464.1	23.93	104.1	1.45	312.7	4.26	146.5	2.49	4	2464.1
06_14	0.16083	0.00184	0.18331	0.00233	4.06525	0.05334	0.02341	0.00036	0.969	2464.4	19.19	1085	12.69	1647.4	10.69	467.7	7.03	44	2464.4
06_18	0.16092	0.00172	0.18489	0.00239	4.10228	0.05303	0.01425	0.0002	1.000	2465.4	17.9	1093.7	13.02	1654.8	10.55	286.1	4.01	44	2465.4
06_36	0.16119	0.00178	0.28889	0.00394	6.4171	0.09005	0.02897	0.00079	0.972	2468.1	18.53	1636	19.7	2034.6	12.33	577.3	15.43	66	2468.1
06_4	0.16142	0.0019	0.30506	0.00434	6.78341	0.09875	0.03956	0.0005	0.977	2470.6	19.78	1716.4	21.43	2083.6	12.88	784.1	9.64	69	2470.6
06_54	0.16161	0.00176	0.33615	0.00465	7.48865	0.10452	0.04317	0.00069	0.991	2472.5	18.29	1868.1	22.45	2171.6	12.5	854.2	13.42	76	2472.5
06_8	0.16173	0.00168	0.2424	0.00309	5.40362	0.06867	0.04892	0.00055	0.997	2473.8	17.41	1399.2	16.01	1885.4	10.89	965.4	10.57	57	2473.8
06_63	0.16176	0.00189	0.28182	0.00378	6.28359	0.08696	0.06733	0.00212	0.969	2474.1	19.56	1600.5	19.02	2016.2	12.12	1317.1	40.14	65	2474.1
06_20	0.16226	0.00177	0.26389	0.0035	5.9038	0.07882	0.02806	0.00044	0.993	2479.3	18.28	1509.7	17.87	1961.8	11.59	559.4	8.62	61	2479.3
06_5	0.16366	0.00174	0.19996	0.00275	4.50901	0.06178	0.02436	0.0003	0.996	2493.9	17.81	1175.1	14.78	1732.6	11.39	486.5	5.84	47	2493.9
06_55	0.16421	0.00177	0.36213	0.00498	8.1974	0.1132	0.05937	0.00081	0.996	2499.4	18.05	1992.3	23.56	2253.1	12.5	1165.7	15.39	80	2499.4
06_24	0.16622	0.0021	0.40191	0.00596	9.20996	0.14199	0.04724	0.00083	0.962	2520	21.03	2177.8	27.43	2359.1	14.12	933	15.95	86	2520
06_29	0.16674	0.00207	0.36954	0.00506	8.49346	0.12303	0.07774	0.00134	0.945	2525.2	20.65	2027.2	23.81	2285.2	13.16	1513.2	25.04	80	2525.2
06_7	0.16694	0.00182	0.39097	0.00529	8.99852	0.12285	0.06844	0.00089	0.991	2527.2	18.21	2127.3	24.52	2337.9	12.48	1338.1	16.87	84	2527.2
06_21	0.16709	0.00361	0.02049	0.00036	0.47166	0.01009	0.00236	0.00011	0.821	2528.7	35.84	130.7	2.26	392.3	6.96	47.6	2.13	5	2528.7
06_61	0.1675	0.00187	0.32889	0.00421	7.59394	0.09937	0.03294	0.00054	0.978	2532.8	18.61	1833	20.43	2184.1	11.74	655	10.6	72	2532.8
06_32	0.16811	0.00185	0.35641	0.00493	8.25824	0.11608	0.05187	0.00108	0.984	2538.9	18.38	1965.1	23.41	2259.7	12.73	1022.2	20.76	77	2538.9
06_60	0.16845	0.00179	0.45877	0.00617	10.65268	0.14322	0.05551	0.00073	1.000	2542.3	17.71	2434.1	27.28	2493.3	12.48	1091.9	14.04	96	2542
06_31	0.16921	0.00211	0.06676	0.00099	1.55731	0.02281	0.00498	0.00027	0.988	2549.8	20.74	416.6	5.95	953.4	9.06	100.5	5.43	16	2549.8

06_12	0.1706	0.00178	0.26254	0.00339	6.17552	0.07939	0.05596	0.0007	0.996	2563.5	17.39	1502.8	17.33	2001	11.23	1100.5	13.44	59	2563.5
06_1	0.17346	0.00199	0.45013	0.00642	10.75144	0.154	0.0547	0.00083	0.996	2591.3	18.97	2395.8	28.55	2501.9	13.31	1076.4	15.94	92	2591
06_34	0.17662	0.00214	0.49334	0.00667	12.01221	0.17058	0.13389	0.00267	0.952	2621.4	20.01	2585.1	28.77	2605.4	13.31	2539.7	47.54	99	2621
06_57	0.17704	0.00207	0.49002	0.00701	11.96077	0.17406	0.09236	0.0015	0.983	2625.3	19.28	2570.8	30.35	2601.3	13.64	1785.6	27.77	98	2625
06_56	0.17841	0.00262	0.01682	0.00025	0.41506	0.00654	0.00191	0.00015	0.943	2638.2	24.17	107.6	1.6	352.5	4.69	38.6	3.13	4	2638.2
06_50	0.18025	0.00219	0.0528	0.00075	1.31166	0.01946	0.00498	0.00008	0.957	2655.2	20.01	331.7	4.62	850.9	8.55	100.4	1.53	12	2655.2
06_30	0.18361	0.00223	0.10978	0.00143	2.77923	0.03872	0.01687	0.00059	0.935	2685.7	19.93	671.5	8.32	1350	10.4	338.1	11.79	25	2685.7
06_58	0.20076	0.00217	0.19561	0.00259	5.41165	0.07167	0.02684	0.0006	1.000	2832.4	17.55	1151.7	13.95	1886.7	11.35	535.4	11.84	41	2832.4
06_46	0.2071	0.00242	0.1034	0.00147	2.94652	0.04257	0.00949	0.00016	0.984	2883	18.85	634.3	8.57	1394	10.95	191	3.13	22	2883
06_3	0.22443	0.00228	0.29787	0.00414	9.21064	0.1244	0.04535	0.00055	0.972	3012.8	16.24	1680.7	20.56	2359.2	12.37	896.4	10.63	56	3012.8
06_16	0.22724	0.00254	0.20966	0.00294	6.56847	0.09207	0.01853	0.00032	1.000	3032.7	17.78	1227	15.68	2055.1	12.35	371.1	6.31	40	3032.7
06_13	0.22882	0.00263	0.14765	0.00195	4.65691	0.06241	0.01394	0.00025	0.985	3043.8	18.32	887.8	10.96	1759.5	11.2	279.9	5.07	29	3043.8
06_52	0.22998	0.00242	0.33502	0.00428	10.62236	0.13399	0.06256	0.0009	0.987	3051.9	16.71	1862.7	20.66	2490.7	11.71	1226.4	17.14	61	3051.9
06_23	0.23022	0.00275	0.17915	0.00266	5.68378	0.08438	0.01516	0.0004	1.000	3053.6	19.02	1062.3	14.52	1928.9	12.82	304.1	7.92	35	3053.6
06_33	0.23119	0.00265	0.32	0.00452	10.19437	0.14557	0.05116	0.00126	0.989	3060.3	18.2	1789.7	22.08	2452.6	13.2	1008.4	24.21	58	3060.3
06_9	0.23739	0.00246	0.62145	0.00868	20.32839	0.27981	0.14611	0.00173	0.985	3102.5	16.41	3115.7	34.53	3107.1	13.32	2756.4	30.52	100	3103
06_17	0.23961	0.0026	0.61297	0.0081	20.24984	0.26614	0.17114	0.00243	0.995	3117.4	17.17	3081.9	32.37	3103.4	12.72	3193.1	41.93	99	3117
06_28	0.23963	0.00268	0.39248	0.00561	12.96659	0.18493	0.03194	0.00056	0.998	3117.5	17.7	2134.3	25.96	2677.2	13.44	635.5	10.9	68	3117.5
06_47	0.24623	0.0025	0.56692	0.00782	19.24357	0.25919	0.1043	0.00125	0.976	3160.7	16.01	2895.2	32.19	3054.1	13	2005.4	22.87	92	3161
06_27	0.24809	0.00254	0.60635	0.00831	20.73585	0.27669	0.11166	0.00144	0.974	3172.6	16.13	3055.4	33.37	3126.3	12.93	2139.6	26.18	96	3173
06_6	0.24933	0.0025	0.54653	0.00709	18.78282	0.23944	0.10343	0.00117	0.983	3180.5	15.78	2810.7	29.56	3030.7	12.29	1989.3	21.41	88	3180.5
06_10	0.25813	0.00264	0.611	0.00801	21.73355	0.28122	0.15019	0.00175	0.987	3235.3	16.01	3074	32.07	3171.9	12.56	2828.2	30.81	95	3235
06_62	0.25823	0.00267	0.52028	0.0069	18.51861	0.24227	0.03246	0.00057	0.986	3235.9	16.2	2700.3	29.26	3017.1	12.6	645.8	11.25	83	3235.9
06_43	0.26635	0.00278	0.53446	0.00736	19.62025	0.26463	0.08915	0.00119	0.979	3284.7	16.27	2760.2	30.9	3072.8	13.03	1726.1	22.07	84	3284.7
06_2	0.27173	0.0028	0.63889	0.00898	23.91322	0.32543	0.08867	0.00117	0.968	3316.1	16.08	3184.6	35.31	3264.9	13.26	1717.1	21.72	96	3316
06_25	0.27184	0.00292	0.2505	0.00326	9.38583	0.12182	0.0255	0.00045	0.997	3316.7	16.71	1441	16.79	2376.4	11.91	509	8.88	43	3316.7
06_44	0.28769	0.00342	0.47266	0.00621	18.75032	0.25572	0.13122	0.00312	0.963	3405.2	18.39	2495.2	27.2	3029.1	13.15	2492.1	55.71	73	3405.2
06_42	0.3041	0.0031	0.61581	0.00843	25.81228	0.3451	0.11263	0.0014	0.977	3491.2	15.7	3093.2	33.65	3339.5	13.07	2157.2	25.43	89	3491.2
06_59	0.3152	0.0035	0.589	0.00768	25.58841	0.33183	0.09258	0.00184	0.995	3546.6	17.01	2985.4	31.17	3330.9	12.67	1789.6	34.09	84	3546.6

CU10-22	Isotope ratios									Ages (Ma)									
Spot name	Pb^{207}/Pb^{206}	± 1 s	Pb^{206}/U^{238}	± 1 s	Pb^{207}/U^{235}	± 1 s	Pb^{208}/Th^{232}	± 1 s	Rho	Pb^{207}/Pb^{206}	± 1 s	Pb^{206}/U^{238}	± 1 s	Pb^{207}/U^{235}	± 1 s	Pb^{208}/Th^{232}	± 1 s	Conc. (%)	Age
CB-1-24	0.06301	0.00417	0.05295	0.00114	0.45956	0.02967	0.01667	0.00096	0.333	708.6	134.69	332.6	6.95	384	20.64	334.2	19.13	46.9	709
CB31	0.08119	0.00141	0.06912	0.00091	0.77369	0.0141	0.02709	0.00043	0.722	1226.1	33.82	430.8	5.51	581.9	8.07	540.2	8.48	35.1	1226
CB34	0.11406	0.00118	0.28633	0.00357	4.50266	0.05668	0.07883	0.00081	0.990	1865	18.57	1623.2	17.89	1731.5	10.46	1533.7	15.11	87.0	1865
CB-1-10	0.12729	0.00163	0.36976	0.0052	6.48834	0.09843	0.08632	0.00127	0.927	2060.9	22.38	2028.3	24.47	2044.3	13.35	1673.4	23.64	98.4	2061
CB-1-4	0.13482	0.00149	0.41876	0.00579	7.78333	0.10928	0.11427	0.00138	0.985	2161.7	19.1	2254.9	26.31	2206.3	12.63	2186.9	25.05	104.3	2162
CB-1-27	0.14839	0.00152	0.31002	0.00418	6.34374	0.08453	0.06522	0.00098	0.988	2327.4	17.43	1740.8	20.59	2024.5	11.69	1277.1	18.56	74.8	2327
CB-1-14	0.15638	0.00157	0.20243	0.00273	4.3643	0.05777	0.03816	0.00043	0.982	2416.9	16.99	1188.4	14.64	1705.6	10.94	756.9	8.46	49.2	2417
CB-1-1	0.15898	0.00177	0.28179	0.00382	6.17416	0.08545	0.08487	0.00105	0.979	2444.8	18.76	1600.4	19.21	2000.8	12.09	1646.4	19.61	65.5	2445
CB-1-16	0.16202	0.00163	0.38219	0.00515	8.53703	0.11257	0.0825	0.00096	0.979	2476.9	16.91	2086.5	24	2289.9	11.98	1602.2	17.97	84.2	2477
CB39	0.1628	0.00171	0.29051	0.00367	6.52075	0.08293	0.08223	0.00099	0.993	2485	17.57	1644.1	18.31	2048.7	11.2	1597.2	18.49	66.2	2485
CB-1-11	0.16293	0.0021	0.45815	0.00654	10.28965	0.15663	0.10683	0.00163	0.938	2486.2	21.58	2431.4	28.93	2461.2	14.09	2051.5	29.84	97.8	2486
CB-1-17	0.16327	0.00177	0.47207	0.00644	10.62528	0.14515	0.10617	0.00125	0.999	2489.8	18.14	2492.6	28.21	2490.9	12.68	2039.5	22.89	100.1	2490
CB-1-6	0.16355	0.00181	0.51018	0.00703	11.50327	0.16075	0.14008	0.0017	0.986	2492.7	18.56	2657.4	30.03	2564.8	13.05	2649.8	30.08	106.6	2493
CB-1-12	0.16357	0.00171	0.47381	0.00645	10.68383	0.1444	0.10549	0.0012	0.993	2492.9	17.52	2500.2	28.21	2496	12.55	2027	21.99	100.3	2493
CB-1-8	0.16369	0.00173	0.46512	0.00637	10.49466	0.14339	0.10471	0.00121	0.998	2494.1	17.71	2462.1	28.02	2479.4	12.67	2012.9	22.13	98.7	2494
CB-1-20	0.16406	0.00194	0.55305	0.00751	12.49919	0.17762	0.1392	0.00257	0.956	2498	19.8	2837.8	31.18	2642.7	13.36	2634.2	45.59	113.6	2498
CB-1-13	0.16412	0.00168	0.48673	0.0066	11.01235	0.14758	0.10895	0.00127	0.988	2498.5	17.17	2556.5	28.62	2524.2	12.47	2090.3	23.11	102.3	2499
CB-1-3	0.16455	0.00176	0.48911	0.0068	11.09663	0.15436	0.12417	0.00136	0.999	2502.9	17.85	2566.8	29.44	2531.3	12.96	2365.8	24.41	102.6	2503
CB-1-19	0.16478	0.00189	0.49879	0.00671	11.32232	0.15769	0.13018	0.00183	0.966	2505.3	19.15	2608.6	28.88	2550	12.99	2473.6	32.81	104.1	2505
CB-1-7	0.165	0.00183	0.47406	0.00664	10.78502	0.15295	0.12051	0.00146	0.988	2507.6	18.55	2501.3	29.05	2504.8	13.18	2299.9	26.4	99.7	2508
CB-1-2	0.16539	0.00179	0.48979	0.00684	11.16846	0.15647	0.12235	0.00139	0.997	2511.6	18.08	2569.8	29.61	2537.3	13.06	2332.9	25.08	102.3	2512
CB38	0.16541	0.00171	0.38322	0.00491	8.73945	0.11222	0.09891	0.00112	0.998	2511.8	17.23	2091.3	22.88	2311.2	11.7	1906.4	20.55	83.3	2512
CB30	0.16593	0.00176	0.43431	0.00543	9.93555	0.1261	0.11222	0.00134	0.985	2517	17.71	2325.1	24.42	2428.8	11.71	2149.7	24.43	92.4	2517

CB28	0.16688	0.00175	0.44036	0.00546	10.1314	0.12687	0.11753	0.00124	0.990	2526.5	17.48	2352.3	24.44	2446.8	11.57	2246	22.51	93.1	2527	
CB36	0.16741	0.00173	0.43886	0.00549	10.12955	0.12749	0.1154	0.00115	0.994	2531.9	17.27	2345.5	24.59	2446.7	11.63	2207.4	20.92	92.6	2532	
CB-1-5	0.16859	0.0019	0.51065	0.00718	11.86998	0.16955	0.13376	0.00175	0.984	2543.7	18.76	2659.4	30.64	2594.2	13.38	2537.4	31.22	104.5	2544	
CB29	0.16882	0.00178	0.43778	0.00549	10.18922	0.12925	0.11645	0.00121	0.989	2545.9	17.53	2340.7	24.63	2452.1	11.73	2226.4	21.83	91.9	2546	
CB-1-23	0.17109	0.00179	0.45182	0.00594	10.64803	0.14079	0.11664	0.00138	0.994	2568.4	17.39	2403.3	26.38	2492.9	12.27	2229.9	24.93	93.6	2568	
CB-1-25	0.17251	0.00199	0.41431	0.00557	9.84464	0.1371	0.12545	0.00177	0.965	2582.2	19.13	2234.6	25.37	2420.3	12.84	2388.8	31.83	86.5	2582	
CB-1-26	0.17329	0.00192	0.49357	0.00657	11.78029	0.16048	0.12799	0.00165	0.977	2589.7	18.36	2586.1	28.35	2587.1	12.75	2434.3	29.58	99.9	2590	
CB-1-18	0.18369	0.00216	0.52766	0.00718	13.35267	0.18852	0.13658	0.00206	0.964	2686.4	19.28	2731.6	30.29	2704.9	13.34	2587.7	36.63	101.7	2686	
CB-1-9	0.21219	0.00211	0.53951	0.00729	15.78072	0.20909	0.12219	0.00143	0.981	2922.3	16.03	2781.4	30.54	2863.6	12.65	2330.2	25.75	95.2	2922	
CB-1-22	0.22604	0.00234	0.37071	0.00487	11.54268	0.15144	0.06523	0.0008	0.999	3024.2	16.48	2032.7	22.91	2568	12.26	1277.2	15.2	67.2	3024	
CB-1-15	0.23529	0.00234	0.62324	0.00839	20.21601	0.26503	0.13318	0.00152	0.974	3088.4	15.77	3122.8	33.32	3101.7	12.68	2527.1	27.18	101.1	3088	
CB37	0.2459	0.00263	0.60274	0.00778	20.43433	0.26544	0.16188	0.00207	0.994	3158.6	16.88	3040.9	31.29	3112.1	12.57	3032.7	35.95	96.3	3159	
CB-1-21	0.2532	0.00293	0.68099	0.00933	23.75216	0.33193	0.16987	0.00226	0.980	3204.9	18.14	3348.2	35.78	3258.3	13.62	3171.2	39.04	104.5	3205	
CB33	0.27413	0.00278	0.57032	0.00709	21.55545	0.26717	0.14711	0.00158	0.997	3329.8	15.79	2909.1	29.11	3163.9	12.03	2774.1	27.9	87.4	3330	
CB32	0.27711	0.0029	0.60731	0.00763	23.20246	0.2924	0.15725	0.00179	0.997	3346.7	16.26	3059.2	30.62	3235.5	12.27	2951.9	31.2	91.4	3347	
CB35	0.28618	0.00312	0.67616	0.0083	26.67659	0.33251	0.164	0.00193	0.985	3397	16.9	3329.6	31.93	3371.7	12.2	3069.5	33.54	98.0	3397	
CB27	0.4777	0.01568	118.5557	31.6101	-	-	-	149.88763	-	4173.8	47.71	-	1704.41	9095.8	270.69	-	-	-	4174	

Table 6.

Analysis No.	Interference Corr. Meth.	Total Hf beam (V)	$^{176}Hf/^{177}Hf$	2 se	exp. factor	2 se	$^{178}Hf/^{177}Hf$	2 se	$^{176}Yb/^{177}Hf$	$^{176}Lu/^{177}Hf$	Age (Ma)	$^{176}Hf/^{177}Hf$ Initial	2 se	$\varepsilon_{Hf}(t)$	T_{DM} (Ga)	T_{DM} Crustal	$^{176}Hf/^{177}Hf$	2 se
CU10-05_04	176Yb	8.379393	0.280769	0.000032	1.028841	0.004000	1.467301	0.000063	0.060120	0.001046	3312	0.280703	1.133915	1.6	3.45	3.54	0.280811	0.000021
CU10-05_05	176Yb	11.467611	0.281119	0.000034	0.991029	0.004479	1.467380	0.000067	0.137047	0.002102	3211	0.280989	1.181902	9.5	3.06	2.96	0.281249	0.000023
CU10-05_09	176Yb	8.932048	0.281296	0.000032	0.777155	0.004013	1.467295	0.000073	0.037424	0.000706	2567	0.281262	1.105796	4.2	2.71	2.81	0.281337	0.000021
CU10-05_11	176Yb	6.722070	0.281084	0.000040	0.806629	0.004727	1.467293	0.000071	0.103429	0.001744	2636	0.280996	1.405010	-3.7	3.08	3.36	0.281225	0.000023
CU10-05_12	176Yb	5.090223	0.281071	0.000036	0.805185	0.004278	1.467307	0.000057	0.111359	0.001898	2623	0.280976	1.267141	-4.7	3.11	3.42	0.281214	0.000022
CU10-05_13	176Yb	9.827435	0.281322	0.000026	1.021568	0.003428	1.467294	0.000052	0.056634	0.000864	2537	0.281281	0.916359	4.2	2.69	2.79	0.281347	0.000018
CU10-05_14	176Yb	8.701761	0.281127	0.000031	1.030303	0.003181	1.467236	0.000050	0.083622	0.001313	3048	0.281050	1.075290	7.8	2.98	2.94	0.281176	0.000019
CU10-05_15	176Yb	7.943073	0.280717	0.000030	0.974423	0.003758	1.467339	0.000054	0.088354	0.001447	3389	0.280623	1.048004	0.6	3.55	3.67	0.280785	0.000018
CU10-05_17	176Yb	8.106071	0.280860	0.000030	0.963038	0.003548	1.467291	0.000056	0.051666	0.000850	3095	0.280809	1.059470	0.4	3.31	3.46	0.280899	0.000020
CU10-05_19	176Yb	7.961604	0.281372	0.000040	0.955518	0.004339	1.467283	0.000076	0.047478	0.000875	3086	0.281320	1.390967	18.3	2.62	2.29	0.281426	0.000024
CU10-05_22	176Yb	8.323498	0.281295	0.000028	0.921796	0.004417	1.467316	0.000059	0.079330	0.001286	2516	0.281233	0.965106	2.0	2.75	2.91	0.281384	0.000019
CU10-22_03	176Yb	5.782124	0.281244	0.000043	0.947733	0.005010	1.467338	0.000087	0.039821	0.000630	2503	0.281214	1.519218	1.0	2.77	2.96	0.281263	0.000026
CU10-22_04	176Yb	6.246762	0.281361	0.000032	0.963233	0.004093	1.467268	0.000058	0.037551	0.000737	2162	0.281331	1.122017	-2.7	2.62	2.94	0.281398	0.000020
CU10-22_05	176Yb	5.809062	0.281156	0.000028	0.962773	0.003416	1.467224	0.000057	0.040130	0.000698	2544	0.281122	0.976883	-1.3	2.90	3.14	0.281221	0.000019
CU10-22_06	176Yb	5.533762	0.281165	0.000034	0.948337	0.004004	1.467256	0.000055	0.014065	0.000293	2493	0.281151	1.178477	-1.4	2.86	3.11	0.281189	0.000024
CU10-22_07	176Yb	7.464262	0.281104	0.000024	0.904169	0.003052	1.467254	0.000050	0.037264	0.000620	2508	0.281074	0.834335	-3.9	2.96	3.28	0.281142	0.000017
CU10-22_09	176Yb	6.279811	0.280874	0.000027	0.898635	0.003316	1.467238	0.000052	0.059581	0.001218	2922	0.280805	0.956303	-3.8	3.32	3.59	0.280948	0.000017
CU10-22_10	176Yb	7.123692	0.281482	0.000026	0.886392	0.003370	1.467267	0.000050	0.044616	0.000750	2061	0.281453	0.893787	-0.7	2.46	2.73	0.281536	0.000016
CU10-22_11	176Yb	5.937893	0.281058	0.000028	0.876799	0.003389	1.467270	0.000049	0.036698	0.000659	2486	0.281027	0.970473	-6.0	3.03	3.40	0.281068	0.000017
CU10-22_12	176Yb	5.691612	0.281149	0.000027	0.875712	0.004190	1.467248	0.000055	0.025715	0.000446	2493	0.281128	0.929968	-2.3	2.89	3.17	0.281191	0.000017
CU10-22_13	176Yb	5.437963	0.281172	0.000034	0.869831	0.004196	1.467286	0.000064	0.025260	0.000431	2499	0.281151	1.179573	-1.3	2.86	3.11	0.281179	0.000023
CU10-22_15	176Yb	8.065264	0.280846	0.000024	0.876112	0.003309	1.467285	0.000049	0.052921	0.000932	3088	0.280791	0.827272	-0.5	3.33	3.51	0.280867	0.000015
CU10-22_17	176Yb	6.447083	0.281281	0.000030	0.866879	0.003718	1.467227	0.000052	0.051653	0.000989	2490	0.281234	1.035371	1.4	2.75	2.93	0.281338	0.000018
CU10-22_19	176Yb	6.804878	0.280861	0.000024	0.883678	0.003369	0.877358	0.025204	0.035887	0.000629	3205	0.280822	0.841851	3.4	3.29	3.35	0.280873	0.000017
CU10-22_23	176Yb	6.333685	0.281077	0.000027	0.869042	0.003628	1.467299	0.000049	0.061749	0.001115	2505	0.281024	0.958816	-5.7	3.04	3.39	0.281170	0.000017
CU10-22_23b	176Yb	3.962320	0.281358	0.000040	0.868746	0.004418	1.467258	0.000060	0.111524	0.002066	2568	0.281256	1.405327	4.0	2.72	2.82	0.281543	0.000024
CU10-22_26	176Yb	6.529082	0.281482	0.000053	0.842627	0.004579	1.467335	0.000085	0.126000	0.001824	2590	0.281392	1.841292	9.3	2.53	2.50	0.281502	0.000033
CU10-22_28	176Yb	5.912499	0.281181	0.000030	0.863945	0.003482	1.467294	0.000057	0.028662	0.000484	2527	0.281157	1.036625	-0.5	2.85	3.08	0.281193	0.000020
CU10-22_29	176Yb	5.571767	0.281232	0.000031	0.871739	0.003497	1.467257	0.000057	0.040264	0.000664	2546	0.281200	1.101389	1.5	2.79	2.97	0.281232	0.000020

Table 7.

Section	Sample	Stratigraphic Height (m)	δ13C VPDB (‰)	δ18O VPDB (‰)
Narji-2	N2-1	7.00	0.74	-12.34
	N2-2	8.70	1.09	-11.68
	N2-3	9.70	1.51	-11.93
	N2-4	12.20	1.40	-10.92
	N2-5	13.80	0.85	-9.26
	N2-6	17.00	1.51	-8.68
	N2-8	18.70	0.24	-7.47
	N2-9	22.00	1.29	-8.02
	N2-10	24.50	1.66	-7.37
	N2-11	28.00	1.35	-7.15
	N2-12	30.50	2.10	-7.11
	N2-13	33.00	1.70	-7.25
	N2-14	35.00	1.09	-7.25
	N2-15	37.50	1.38	-7.30
	N2-16	40.00	0.20	-7.31
	N2-17	42.50	1.11	-6.98
	N2-18	45.00	1.62	-6.80
	N2-20	50.00	1.48	-7.64
	N2-21	52.50	1.63	-7.61
	N2-22	55.00	2.10	-7.08
	N2-23	57.20	1.98	-7.66
	N2-24	60.00	1.73	-6.89
	N2-25	62.50	1.22	-7.78
	N2-26	65.00	1.81	-7.23
	N2-27	67.50	1.56	-8.28
	N2-28	70.00	2.03	-7.71
	N2-29	72.50	2.47	-9.07
	N2-30	75.00	2.34	-9.37
	N2-31	77.50	2.16	-9.09
	N2-32	80.00	1.51	-10.35
	N2-33	82.50	1.62	-8.86
	N2-34	85.00	1.52	-10.50
	N2-35	87.50	1.82	-9.92
Narji-3	N3-1.0	1.0	2.41	-9.30
	N3-1.5	1.5	1.90	-9.82
	N3-2.0	2.0	2.01	-9.69
	N3-3.0	3.0	2.02	-9.73
	N3-3.9	3.9	1.90	-9.81
	N3-5.5	5.5	1.40	-10.19
	N3-6.4	6.4	1.64	-10.49
	N3-8.0	8.0	1.72	-10.29
	N3-8.5	8.5	1.45	-10.83